


High-quality evergreen azalea genome reveals tandem duplication-facilitated low-altitude adaptability and floral scent evolution

Xiuyun Wang^{1,†}, Yuan Gao^{2,†}, Xiaopei Wu^{3,†}, Xiaohui Wen¹, Danqing Li¹, Hong Zhou¹, Zheng Li¹, Bing Liu¹, Jianfen Wei⁴, Fei Chen⁵, Feng Chen⁶, Chengjun Zhang^{3,*}, Liangsheng Zhang^{1,*} and Yiping Xia^{1,*} 

¹Genomics and Genetic Engineering Laboratory of Ornamental Plants, College of Agriculture and Biotechnology, Zhejiang University, Hangzhou, China

²Fujian Provincial Key Laboratory of Haixia Applied Plant Systems Biology, Key Laboratory of Ministry of Education for Genetics & Breeding and Multiple Utilization of Crops, College of Life Science, Fujian Agriculture and Forestry University, Fuzhou, China

³The Southwest China of Germplasm Bank of Wild Species, Kunming Institute of Botany, Chinese Academy of Sciences, Kunming, China

⁴Research & Development Center, Hangzhou Landscaping Incorporated, Hangzhou, China

⁵College of Horticulture, Nanjing Agricultural University, Nanjing, China

⁶Department of Plant Sciences, University of Tennessee, Knoxville, TN, USA

Received 17 December 2020;

accepted 27 July 2021.

*Correspondence (Tel 86-0571-88982391; email ypxia@zju.edu.cn (YX); Tel 86-17720805596; email zls83@zju.edu.cn (LZ); Tel 86-0871-65230892; email zhangchengjun@mail.kib.ac.cn (CZ))

[†]These authors contributed equally to this work.

Summary

Azalea belongs to *Rhododendron*, which is one of the largest genera of flowering plants and is well known for the diversity and beauty in its more than 1000 woody species. *Rhododendron* contains two distinct groups: the most high-altitude and a few low-altitude species; however, the former group is difficult to be domesticated for urban landscaping, and their evolution and adaptation are little known. *Rhododendron ovatum* has broad adaptation in low-altitude regions but possesses evergreen characteristics like high-altitude species, and it has floral fragrance that is deficient in most cultivars. Here we report the chromosome-level genome assembly of *R. ovatum*, which has a total length of 549 Mb with scaffold N50 of 41 Mb and contains 41 264 predicted genes. Genomic micro-evolutionary analysis of *R. ovatum* in comparison with two high-altitude *Rhododendron* species indicated that the expansion genes in *R. ovatum* were significantly enriched in defence responses, which may account for its adaptability in low altitudes. The *R. ovatum* genome contains much more terpene synthase genes (TPSs) compared with the species that lost floral fragrance. The subfamily b members of TPS are involved in the synthesis of sesquiterpenes as well as monoterpenes and play a major role in floral scent biosynthesis and defence responses. Tandem duplication is the primary force driving expansion of defence-responsive genes for extensive adaptability to the low-altitude environments. The *R. ovatum* genome provides insights into low-altitude adaptation and gain or loss of floral fragrance for *Rhododendron* species, which are valuable for alpine plant domestication and floral scent breeding.

Keywords: Azalea, *Rhododendron ovatum*, altitude, adaptability, floral scent, terpene synthase (TPS), tandem duplication, defence response.

Introduction

The genus *Rhododendron* comprises one of the largest and most diverse groups of woody ornamental plants in cultivation, ranging from spectacular trees to evergreen or deciduous shrubs and alpine cushions (Cameron, 1993; De Riek *et al.*, 2018). *Rhododendron* plants have attractive foliage and flowers, which in some species are sweetly fragrant, and are economically important as ornamental landscapes or pot plants (De Riek *et al.*, 2018; Norton and Norton, 1989). The genus *Rhododendron* contains more than 1,000 species. Because of the large number of the species in this genus, taxonomists have made several classifications based on morphology, now the most universally accepted classification system subdivides the genus *Rhododendron* into eight subgenera, including the five most important subgenera: *Rhododendron*, *Hymenanthes*, *Azaleastrum*, *Tsutsusi*, and *Pentanthera* (Chamberlain *et al.*, 1996). The former two subgenera comprise what gardeners loosely refer to as 'rhododendrons', whereas the latter

three subgenera comprise the 'azaleas' (Figure 1a) (De Riek *et al.*, 2018). The evolution and adaptation of the two different groups, high-altitude rhododendron and low-altitude azalea of this genus, remain largely unexplored.

The species of rhododendron group account for a large portion of the genus and possess diverse fascinating flowers. However, evergreen rhododendrons prefer to grow in cool and humid forest environments with acidic soil in the alpine or subalpine zone, which shows a temperate climate even in the tropics or subtropics. Thus, high-altitude rhododendrons can hardly adapt to the hot and dry urban summer environment during domestication. Another group azaleas distribute in low altitudes and are widely cultivated and applied in urban landscapes. The azalea group contains evergreen, semi-evergreen, and deciduous species, of which the subgenus *Azaleastrum* species all have evergreen characteristics like high-altitude rhododendrons but mainly distributed at low altitudes of approximately 300–2000 m (Figure 1a). Moreover, the evolutionary position of *Azaleastrum*

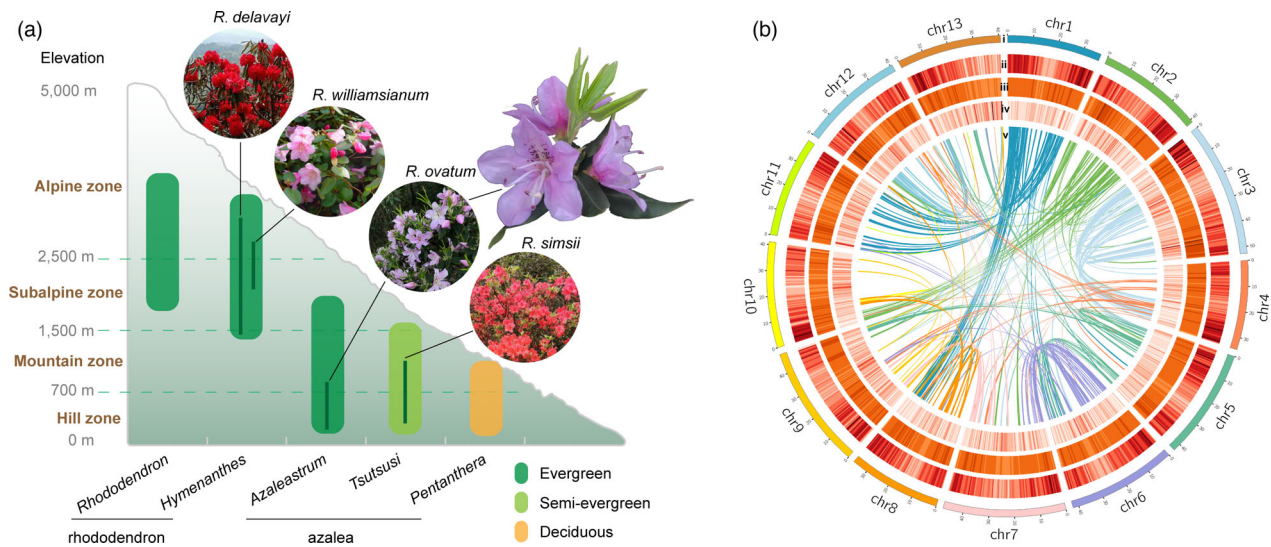


Figure 1 Characteristics of *Rhododendron ovatum* and its genome assembly. (a) Low-altitude and evergreen characteristics of *R. ovatum*. The genus *Rhododendron* contains five main subgenera, of which two subgenera (*Rhododendron* and *Hymenanthes*) commonly called 'rhododendron' are mainly distributed in alpine and subalpine zone, and the other three (*Azaleastrum*, *Tsutsusi*, and *Pentanthera*) commonly called 'azalea' are distributed in mountain and hill zone. The subgenera of *Rhododendron*, *Hymenanthes*, and *Azaleastrum* are mostly evergreens, while *Tsutsusi* are mainly semi-evergreens and *Pentanthera* are deciduous. Genome sequences of *R. delavayi* and *R. williamsianum* in subgenus *Hymenanthes*, and *R. simsii* in subgenus *Tsutsusi* were previously reported (Soza *et al.*, 2019; Yang *et al.*, 2020; Zhang *et al.*, 2017a). (b) Overview of the *R. ovatum* genome assembly. (i) The 13 pseudochromosomes, (ii) gene density, (iii) transposon elements, (iv) tandem repeats, and (v) collinear blocks of the *R. ovatum* genome.

in the genus *Rhododendron* has been proposed with different points. According to morphological classification, the evolutionary process of the genus *Rhododendron* was deduced from evergreen to semi-evergreen and deciduous plants, and the subgenus *Azaleastrum* has a transitional evolutionary position that links rhododendrons and azaleas (Ming and Fang, 1990). In another report, *Azaleastrum* was supported to be the early subgenus that diverged from *Rhododendron* ancestor based on the dated molecular phylogeny using nine chloroplast genes and seven nuclear regions (Shrestha *et al.*, 2018). Therefore, the subgenus *Azaleastrum* has important position for evolution and adaptation in the genus *Rhododendron*. To date, there are two draft genomes for *R. delavayi* (Zhang *et al.*, 2017a) and *R. williamsianum* (Soza *et al.*, 2019) in subgenus *Hymenanthes*, and a genome assembly for the semi-evergreen *R. simsii* in subgenus *Tsutsusi* was newly published (Yang *et al.*, 2020). However, no genome sequencing was reported for the important subgenus *Azaleastrum*. Genome-wide analysis of the species in *Azaleastrum* will contribute to elucidating its evolutionary position and adaptive mechanisms between high-altitude rhododendrons and low-altitude azaleas.

Floral scent is one of the most important trait for ornamental plant and has been always the breeding objective for *Rhododendron* cultivars (Kobayashi *et al.*, 2008). In the large genus *Rhododendron*, only a small amount of species has floral scents, and the fragrant flowers generally exhibit light or faded colours like white, cream, pink or pale yellow (Cameron, 1993). Floral scents comprise complex compound with over 1700 volatile compounds have been identified from nearly 1000 species of flowering plants, which mainly belong to three compound classes of terpenes, benzenoids and fatty acid derivatives (Knudsen *et al.*, 2006). Floral scent constitutes an ancient and important channel of communication between flowering plants and their pollinators

or enemies, and important for the understanding of adaptations and evolutionary processes of angiosperms (Raguso, 2008). Orchidaceae are by far the best-investigated family for floral scent, followed by several families, such as Araceae, Arecaceae, Magnoliaceae and Rosaceae (Knudsen *et al.*, 2006). However, the compounds and evolution of floral scents of *Rhododendron* plants are still poorly investigated.

To fill the gaps in adaptation and floral scents of *Rhododendron* plants, we present a high-quality reference genome of *Rhododendron ovatum* (Lindl.) Maxim., the representative species of subgenus *Azaleastrum*, using PacBio sequencing and Hi-C technology. *R. ovatum* is an evergreen shrub or a small tree that is widely distributed in subtropical zones with altitudes <1000 m (Figure 1a) (Zhang *et al.*, 2017b). In addition to its extensive adaptability, *R. ovatum* possesses white to pink or pinkish purple corolla, often with dark purple spots in the upper part, and has pleasant fragrance, which shows a fine combination of flower coloration and aroma. We performed comparative genomic analysis between *R. ovatum* and two high-altitude rhododendrons to elucidate their micro-evolutionary differences in low-altitude adaptation. Analyses of biosynthesis pathways and key genes of the floral scent compounds elucidated evolution path of floral fragrance in *Rhododendron* species and provided candidate genes for breeding. This genomic study of *R. ovatum* will provide a better understanding of the evolution and adaptation of *Rhododendron* and make more contributions to evolutionary research on Ericales.

Results

Genome sequencing, assembly and annotation

The genome size of the *R. ovatum* was estimated to be 529 Mb with an extremely high heterozygosity of 1.55% based on *k*-mer

analysis of 76 Gb of clean short reads (~144-fold coverage) (Figure S1A, Table S1). For genome sequencing, we obtained a total of 56.7 Gb of PacBio long-read sequencing data, which represents ~107-fold coverage of the estimated genome (Table S2), using single-molecule real-time (SMRT) sequencing technology. We initially assembled the PacBio reads into contig sequences of 712 Mb using Falcon/Falcon-Unzip (Chin *et al.*, 2016) and polished them using Arrow (Table S3). The redundant sequences from heterozygous genomic regions were filtered out using purge_haplotigs (Figure S1B, C; Table S4) (Roach *et al.*, 2018), and the contig sequences were further polished using short reads. This yielded a genome assembly of 549 Mb with a contig N50 length of 1.24 Mb, and the longest contig is 7.45 Mb (Table 1, Table S3). A total of 64.5 Gb of clean reads (Table S5) were generated during construction of the Hi-C sequencing library. This enabled 99.05% of the assembled sequences to be anchored onto 13 pseudo-chromosomes ($2n = 26$) (Figure 1b), which could be well distinguished in the chromatin interaction heatmap (Figure S2). The final chromosome-level genome assembly of *R. ovatum* was 549 Mb with a scaffold N50 of 41 Mb, which has higher integrity and continuity than that of the other three *Rhododendron* species (scaffold N50: 36, 0.6, and 29 Mb, separately) (Table 1).

To provide RNA-level evidence for genome annotation, we generated 147.8 Gb of PacBio ISO-seq subreads (Table S6) obtained from three tissue types (stem, leaf and flower) and finally got 269 Mb of high-quality, full-length and consistent isoform sequences after processing. In combination with ab initio-, homologous- and ISO-seq-based predictions, we identified 41,264 protein-coding genes in the *R. ovatum* genome, which is greater than other sequenced species in Ericales except in tea plant (*Camellia sinensis*) (Table 1, Table S7). Of these protein-coding genes, 39,405 were annotated with known proteins. We identified 245.48 Mb (44.71%) of repetitive sequences, and long

terminal repeat (LTR) retrotransposons accounted for 28.42% of the entire genome (Table S8). A total of ~158 037 simple sequence repeats were annotated (Table S8), which will provide valuable molecular markers to assist azalea breeding. Genome comparison between *R. ovatum* and *R. williamsianum* indicated that more genes and tandem repeats were identified in the former (Figure S3), indicating a higher quality of annotation for the *R. ovatum* genome.

The completeness of the *R. ovatum* genome assembly was evaluated using the Benchmarking Universal Single-Copy Orthologs (BUSCO) gene sets and available ISO-seq data. BUSCO analysis showed that 96.4% of the core eudicotyledon genes are present in the *R. ovatum* genome, of which 95.3% had complete coverage (Table S9), higher than that of *R. simsii* (93.7%), *R. delavayi* (92.8%), *R. williamsianum* (89.0%) and most other sequenced genomes in Ericales (Table 1). In addition, 269 Mb of polished PacBio ISO-seq data were mapped onto the *R. ovatum* genome assembly and showed a high mapping rate of 99.66%. LTR annotation showed an LTR assembly index (LAI) score of 18.32, which meets the reference quality ($10 \leq \text{LAI} < 20$) and is higher than that of tea plant (*Camellia sinensis*) (12.45) and *R. simsii* (18.10) (Xia *et al.*, 2020; Yang *et al.*, 2020). In summary, the extensive coverage of core eudicotyledon genes, high mapping rate of ISO-seq reads and the high LAI score that represents reference genome quality indicated the high completeness and accuracy of the assembled genome. Moreover, our gene predictions covered 96.10% of highly conserved core proteins in the eudicot lineage, which is much higher than that of the other three *Rhododendron* genomes (89.91%, 87.40% and 77.20%, separately) and most other plants in Ericales (Table 1, Table S10). Overall, the evaluations demonstrated that the *R. ovatum* genome has superior quality in assembly and annotation among the reported plants in *Rhododendron* and Ericales.

Table 1 Comparisons of genome assemblies and annotations among species in the Ericales

Species	Assembled genome size (Mb)	Contig N50 (kb)	Scaffold N50 (kb)	Complete BUSCOs of assembly (%)	Annotated gene numbers	Complete BUSCOs of annotation (%)	Repetitive sequences ratio (%)	Reference
<i>Rhododendron ovatum</i>	549	1241	41 000	95.30	41 264	96.10	44.70	This study
<i>Rhododendron simsii</i>	529	2235	36 351	93.68	32 999	89.91	47.48	Yang <i>et al.</i> (2020)
<i>Rhododendron delavayi</i>	695	62	638	92.80	32 938	87.40	51.77	Zhang <i>et al.</i> (2017a)
<i>Rhododendron williamsianum</i>	532	219	29 011	89.00	23 559	77.20	58.80	Soza <i>et al.</i> (2019)
<i>Vaccinium corymbosum</i>	1680	15	186	95.50	32 140	97.21	44.31	Colle <i>et al.</i> (2019)
<i>Actinidia chinensis</i>	654	1430	20 000	90.80	38 202	86.33	43.42	Wu <i>et al.</i> (2019)
<i>Primula vulgaris</i>	411	1	295	89.92	24 000	86.23	37.03	Cocker <i>et al.</i> (2018)
<i>Diospyros lotus</i>	746	1060	29 749	78.97	40 532	74.07	66.60	Akagi <i>et al.</i> (2020)
<i>Camellia sinensis</i>	2940	600	167 113	90.60	50 525	90.24	86.87	Xia <i>et al.</i> (2020)

Whole-genome duplication of *R. ovatum*

Whole-genome duplication (WGD) has been considered as an important factor for genome evolution (Moriyama and Koshiba-Takeuchi, 2018). To investigate the WGD events during the evolution of *R. ovatum*, gene duplications were searched and classified into four types, among which WGD/segmental duplication covered 8027 genes (18.4%) (Figure S4). We characterized the distribution of the synonymous substitution rate (K_s) based on the collinear gene pairs of *R. ovatum* and other species, including kiwifruit (*Actinidia chinensis*), *C. sinensis* and *R. williamsianum* from Ericales, as well as tomato (*Solanum lycopersicum*) and grape (*Vitis vinifera*) from eudicots (Figure 2a). Our results confirmed that an ancient whole-genome triplication (WGT, $At-\gamma$, K_s peak value = 1.43), which is shared by core eudicots (Badouin *et al.*, 2017), and a recent WGD ($Ad-\beta$, K_s peak value = 0.63), which is shared by some families within Ericales (Zhang *et al.*, 2020a), had occurred during the evolutionary history of *R. ovatum*. The occurrence time of $Ad-\beta$ is close to that of the triplication event (Solanaceae- T) of tomato. Moreover, kiwifruit had experienced another recent WGD ($Ad-\alpha$) in addition to $Ad-\beta$, which is consistent with previous reports (Huang *et al.*, 2013; Shi *et al.*, 2010).

To further elucidate the WGD of *R. ovatum* genome, we performed K_s dot plot (Figure 2b) based on the K_s value of paralogues inherited from $Ad-\beta$ (blue dots) and $At-\gamma$ (red dots) using TBtools (v 1.074) (Chen *et al.*, 2020). The $Ad-\beta$ paralogues shows obvious 1:1 diagonal relationships between Chr1:Chr11, Chr2:Chr10, Chr3:Chr4, Chr6:Chr7, etc. Furthermore, K_s peak boundaries corresponding to $Ad-\beta$ (0.20–1.05) and $At-\gamma$ (1.05–2.46) were derived from Gaussian mixture modelling (Teh *et al.*, 2017). We illustrated the intra-genomic synteny blocks among chromosomes 1, 8 and 11 of *R. ovatum*, and the syntenic gene pairs based on K_s peak boundaries showed the retained genes that were derived from $Ad-\beta$ (blue lines, K_s mean = 0.71) and $At-\gamma$ (red lines, K_s mean = 1.59) (Figure 2c). In addition, K_s dot plot of retained orthologues of *R. ovatum*-*V. vinifera* (Figure S5) and *R. ovatum*-*A. chinensis* (Figure S6) supported the recent $Ad-\beta$ and $Ad-\alpha$ events, respectively. These data further supported the occurrence of the recent WGD event ($Ad-\beta$) in *R. ovatum* followed by extensive gene loss.

Phylogenetic placement of *R. ovatum*

To explore the genome evolution of *R. ovatum*, genes of eight species from Ericales with tomato were clustered into 28 190 orthologous groups (OGs) (Data S1). Of these, 380 single-copy orthologues were identified and used to reconstruct a phylogenetic tree (Figure 3a). According to the phylogenetic tree, *R. ovatum* (subgenus *Azaleastrum*) diverged from *Rhododendron* ancestor around 11.85 million years ago (MYA), and *R. simsii* (subgenus *Tsutsusi*) diverged from ancestor of *R. delavayi* and *R. williamsianum* (subgenus *Hymenanthes*) 10.59 MYA. The divergence time between the *R. delavayi* and *R. williamsianum* was estimated to be about 6.95 MYA. Thus, subgenus *Azaleastrum* diverged earlier than *Tsutsusi*, followed by *Hymenanthes*. However, the evolutionary distance between *R. ovatum* and *Hymenanthes* is less than that between *R. simsii* and *Hymenanthes*, indicating that *R. ovatum*, compared with *R. simsii*, has less genetic variance with *Hymenanthes*. Moreover, *R. ovatum* has least genetic variance from *Rhododendron* ancestor among these four *Rhododendron* species. These genetic variance relationships are in accord with morphological characteristic differences

among *Azaleastrum*, *Tsutsusi* and *Hymenanthes*. Taken together, *R. ovatum* had early divergence but conservative evolution, which probably make it most similar to the *Rhododendron* ancestor.

Expansion of stress-responsive genes related to low-altitude adaptability

The four *Rhododendron* species have various genetic expansion and contraction patterns (Figure 3a). To identify the differential evolution and adaptation between low-altitude evergreen *R. ovatum* and the two high-altitude evergreen rhododendrons, a total of 394 expanded OGs were determined in *R. ovatum* compared with *R. delavayi* and *R. williamsianum*. Gene Ontology (GO) term enrichment analyses of the expanded genes demonstrated that a large number of genes were involved in responses to biotic stresses (insect, nematode, fungus and virus), abiotic stresses (nitrogen compound, water deprivation, hypoxia, acidic pH and toxin) and hormones (salicylic acid and jasmonic acid) (Figure 3b, Data S2). Some of these gene families, such as cytochrome P450 (*CYP450*), *MYB*, ethylene-responsive factor (*ERF*), *NAC* and terpene synthase (*TPS*), are related to more than one GO term, indicating their multiple functions in defence responses. Gene members of the transcription factors *MYB*, *ERF* and *NAC* were identified and used to construct phylogenetic trees to explore their evolutionary significance of lineage-specific duplications in *R. ovatum* (Figure 3c, Figures S7 and S8). Most of the expanded genes in the three gene families of *R. ovatum* show uniformly dispersed individual duplication, except one of the *NAC* subfamily *ANAC001*, which was densely expanded with 39 genes in *R. ovatum*, much higher than that in *R. delavayi* and *R. williamsianum* (12 and 4 genes, respectively) (Figure 3c, Figure S9). Chromosome localization of *NAC* genes demonstrated that most of the members in the *ANAC001* clade show tandem repeats on chromosomes 7, 9, 11, 12 and 13 (Figure S10). In particular, 9 and 11 copies are densely distributed on chromosomes 7 and 12 across stretches of 90 kb and 152 kb, respectively (Figure 3c). In addition, 2, 9 and 4 genes experienced positive selection ($K_a/K_s > 1$) of *MYB*, *ERF* and *NAC*, respectively, in *R. ovatum* compared to either *R. delavayi* or *R. williamsianum* (Figure 3c, Figures S7 and S8). Based on the weighted gene co-expression network analysis (WGCNA) of the transcriptomes (Figure S11), the transcription factors *NAC*, *MYB*, *WRKY*, *HSF* and *bZIP*, and the structural proteins *CYP450*, *UGT*, *PP2*, *PDR* and chitinase were found in the co-expression network of an *NAC* member (*Ro_40853*), which is highly expressed in leaf, stem and flower tissues of *R. ovatum* (Figure 3d). We revealed that *NAC* genes are likely critical transcriptional factors in regulating massive stress-responsive genes involved in extensive adaptability of *R. ovatum* in the complex environments of low-altitude areas.

In consideration of temperature as a major factor in low-altitude environments compared with high altitude, the responses of the expanded gene families mentioned above to medium (37°C) and severe (42°C) heat stress were investigated. Among these gene families, some members of *HSP70s* and *TPSs* had elevated transcript abundance after medium or severe heat stress (Figure S12), which indicates their involvement in the temperature response besides the GO-enriched responses above. In addition, *HSFs*, which serve as the master transcriptional regulators in response to heat stress, were identified in *R. ovatum* and compared with the two rhododendrons. Phylogenetic analysis showed that the *HSF* family of *R. ovatum* has duplications in subfamilies of *A2*, *A4*, *A6* and *A9*. Moreover, *HSFA2*, *A4*, *A7* and *B1* exhibited significant responses to heat stress (Figure S13).

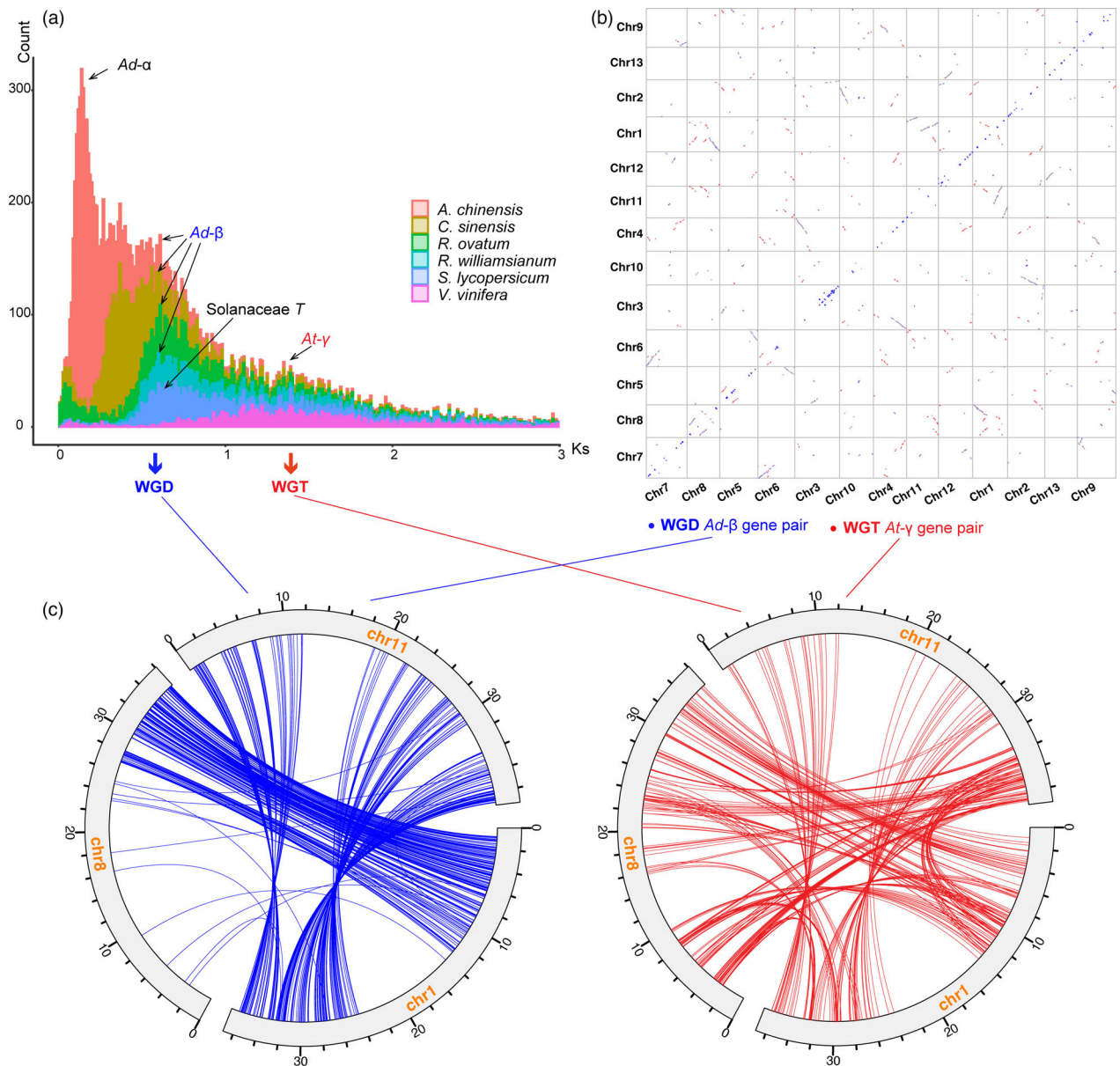


Figure 2 Whole-genome duplication (WGD) events of *R. ovatum*. (a) The synonymous substitution rates (Ks) distributions of paralogous genes in *A. chinensis*, *C. sinensis*, *R. ovatum*, and *R. williamsianum* of the Ericales, and the other two core eudicot plant *S. lycopersicum* and *V. vinifera*. (b) Ks dot plot based on Ks value of *R. ovatum* syntenic gene pairs. (c) Inter-genomic synteny blocks among chromosomes 1, 8, and 11 of *R. ovatum*. The blue and red lines indicate the retained genes that were derived from *Ad-β* and *At-γ* events, respectively.

Tandem duplication had critical effects on the expansion of NAC genes. In addition, it has been reported that expanded genes generated by tandem duplication exhibited important roles in responses to various environmental stimuli (Dassanayake *et al.*, 2011; Hanada *et al.*, 2008). Thus, we performed analyses of relationships between tandem duplication and gene functions. First of all, the ratios of tandem duplication in all types of duplication of the four *Rhododendron* species were investigated, and we found that *R. ovatum* has a higher duplication ratio (20.21%) compared with that of *R. simsii* (14.39%), *R. delavayi* (12.37%) and *R. williamsianum* (11.96%) (Figure S14A). All the tandem-duplicated genes of *R. ovatum* were extracted, and their Pfam domains were annotated and ranked with target gene

numbers. The top 20 Pfam domains contained in the hundreds of tandem-duplicated genes include protein tyrosine kinase (489 genes), leucine-rich repeat (325), F-box domain (210), cytochrome P450 (184), UDP-glucuronosyl and UDP-glucosyltransferase (182), NB-ARC domain (178), ankyrin repeats (117) and PPR repeat family (104) (Figure S14B and Data S5).

To deeply understand the roles of tandem duplication in the evolutionary process of *R. ovatum*, GO annotation and enrichment of all the tandem-duplicated genes were also performed. For the biological processes, more downstream GO terms were significantly enriched (corrected *P*-value < 0.05) compared with upstream GO terms in the hierarchical structure of the network (Figure S15 and Data S6). The most enriched group is related to

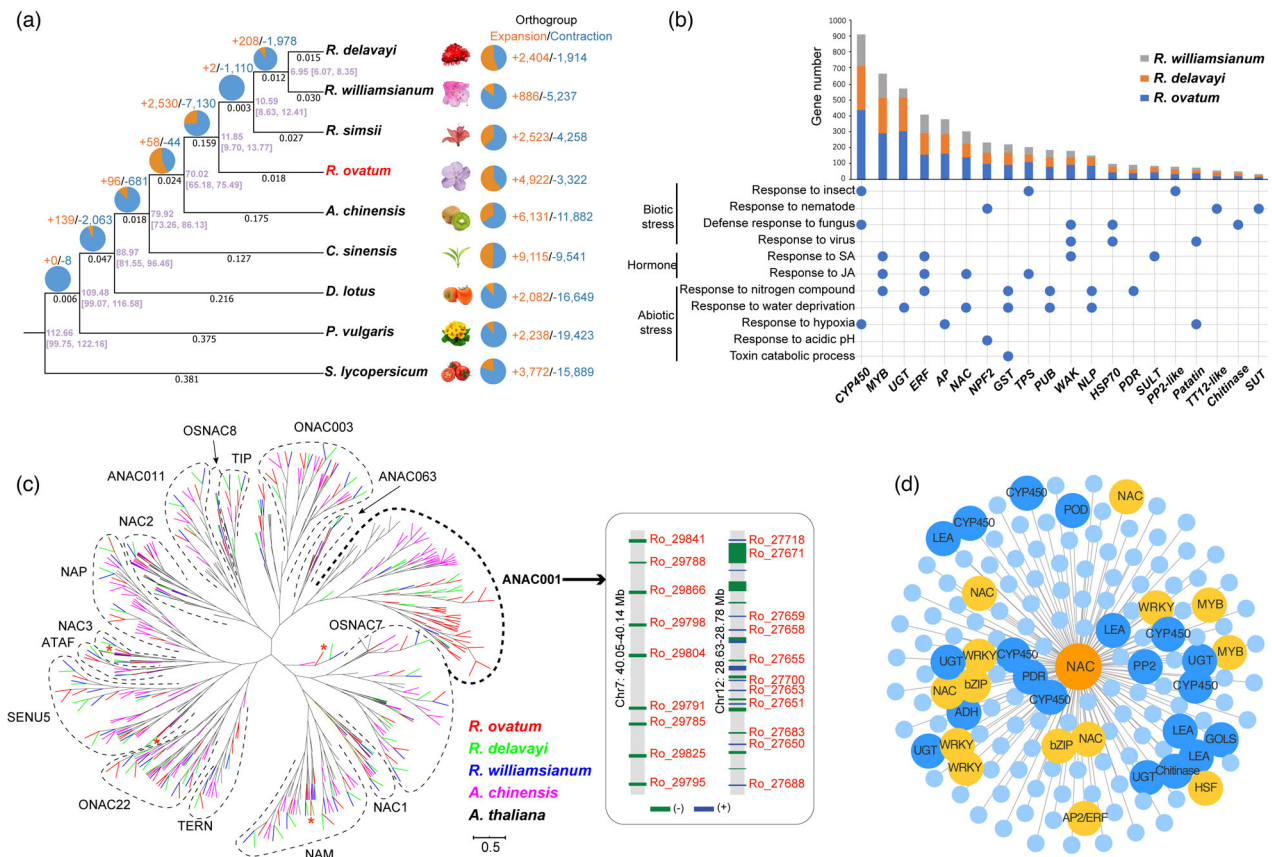


Figure 3 Phylogenetic relationship and comparative genomics analyses. (a) Phylogenetic tree based on single-copy genes from 8 plant species in the Ericales, and tomato (*S. lycopers*) was used as the outgroup. The numbers in purple beside each node shows the estimated divergent time of each node (myr), and those in brackets are 95% confidence intervals for the time of divergence between different clades. The pie diagram on each branch of the tree represents the proportion of orthogroups undergoing gain (orange) or loss (blue) events, and the numbers beside the pie diagram denote the total number of expansion and contraction orthogroups. The numbers under each branch indicate evolutionary distance that represent genetic variance. (b) Gene expansions in *R. ovatum* compared to *R. delavayi* and *R. williamsianum*. Left panel shows enriched GO terms of expansive genes related to stress responses. Bottom and up panels show the names and gene numbers of the expansive gene families involved in the GO terms. The dots indicate corresponding relations between GO terms and gene families. The full names of gene families are listed in Data S3. (c) The phylogenetic tree of NAC genes from *R. ovatum* and representative plants showing the extremely expanded clade of ANAC001 in *R. ovatum*. Branches are colour-coded according to species. Asterisks (*) indicate the genes that have undergone positive selection ($Ka/Ks > 1$). Right panel shows dense tandem arrays of ANAC001 members that are distributed on chromosomes 7 and 12 of *R. ovatum*. (d) Co-expression network analysis based on a highly expressed NAC gene member (*Ro_40853*). Orange circles represent transcription factors and blue circles represent structural proteins.

stimulus responses, including biotic stresses (virus, insect and bacterium), chemical stimulus, singlet oxygen, organic nitrogen, growth hormone and indolebutyric acid. In addition, immune response, glutathione and xyloglucan metabolic processes, toxin catabolic process, terpene and steroid metabolic processes, which were involved in defence responses, were also significantly enriched. Other enrichments are small molecule (organic acid and carboxylic acid) biosynthetic process, auxin transport, pollination and pollen tube growth, regulation and negative regulation of peptidase activity. These results indicated that most functions of the tandem-duplicated genes are related to defence responses. Furthermore, we investigated the proportions of tandem duplication of the above-mentioned expansive genes in Figure 3b. The results showed that 15 of 20 gene families exhibited higher tandem duplication ratio than the average level (20.21%) of the whole genome (Figure S16), indicating a primary contribution of tandem duplication for expansion of these stress-responsive genes.

Flora scent and biosynthesis pathways of the volatiles in *R. ovatum*

Floral fragrance is one of the most important objectives in evergreen azalea breeding (Kobayashi *et al.*, 2008). However, in the genus *Rhododendron*, only a few species have flower fragrance, and most of the cultivated azaleas are short of the attractive trait. *R. ovatum* flowers have pleasant aroma, and the flora volatile organic compounds (VOCs) were analysed using headspace collection combined with GC-MS (Figure 4a, Table S11). Terpenes and fatty acids are the two main classes of VOCs that were detected. The terpenes include three monoterpenes (3-carene, linalool and L- α -terpineol), one sesquiterpene (α -farnesene) and one triterpene (squalene), among which α -farnesene had the highest content. The fatty acids include tetradecanoic acid (14:0), palmitoleic acid (16:1), n-hexadecanoic acid (16:0), 6-octadecenoic acid (18:1) and

octadecanoic acid (18:0). Other components with lower contents, such as methyl cinnamate, elemicin and isopropyl myristate, were also detected. With the identification of scent compounds from *R. ovatum* flowers, next we analysed the genes in the respective biosynthetic pathways.

In green plants, two canonical pathways are involved in the biosynthesis of terpenes: the mevalonic acid (MVA) pathway in the cytosol for sesquiterpene and triterpene biosynthesis and the methylerythritol phosphate (MEP or non-mevalonate) pathway in plastids for monoterpene, diterpene and tetraterpene biosynthesis (Chen *et al.*, 2011; Gershenzon and Kreis, 1999). In the present study, the genes involved in both pathways were isolated, and their expression levels were evaluated and compared between the tissues of leaves, stems and flowers (Figure 4b). TPSs are the key enzymes responsible for biosynthesis of terpenoid compounds, which are also involved in significantly expanded genes in *R. ovatum* compared to the two rhododendrons (Figure 3b). The TPSs (Ro_38431 and Ro_43236) with plastid transit peptides and high gene expression in flowers probably play important roles in monoterpene synthesis in plastids related to flower fragrance and those without plastid transit peptides (Ro_42833, Ro_43201, Ro_43281) probably contribute to sesquiterpene biosynthesis in the cytosol. Key genes encoding the enzymes in the pathway for biosynthesis of steroids, a subclass of terpenoids, are also enriched in the GO terms of expanded genes (Data S2). High expression of squalene monooxygenase (SQLE) and UDP-glycosyltransferase (UGT) in flowers may facilitate steroid synthesis derived from squalene. It is noteworthy that abundant CYP450 could result in the structural diversity of terpene derivatives, especially triterpenoid saponins

(Seki *et al.*, 2015). Thus, given that its three alternative transcripts all exhibited significant expression in flowers, the *CYP450* gene member Ro_40248 is probably a key player in the metabolism of triterpenes (Figure 4b, Figure S17).

Fatty acid derivatives in flower VOCs are mainly esters, alcohols, aldehydes and ketones (Knudsen *et al.*, 1993). It is rare to observe free fatty acids (Knudsen *et al.*, 1993), despite their occurrence in abundance in some flowers such as *Hydnora Africana* (Burger *et al.*, 1988). It is very interesting that five fatty acids, including saturated 14:0, 16:0 and 18:0, and unsaturated 16:1 and 18:1, were detected in the flower VOCs of *R. ovatum* (Figure 4a). In the fatty acid biosynthesis pathway, fatty acyl-acyl carrier protein (ACP) thioesterases play an essential role in chain termination during *de novo* fatty acid synthesis, hence determining the amount and type of free fatty acids that are exported from the plastids for regulating lipid metabolism (Bonaventure *et al.*, 2003; Jones *et al.*, 1995). There are two different classes of fatty acyl-ACP thioesterases described in plants: FatA and FatB (Salas and Ohlrogge, 2002). FatAs exhibit the highest activity for 18:1-ACP and much lower activity for saturated acyl-ACPs, whereas FatBs prefer saturated acyl-ACP substrates but also have activity for unsaturated acyl groups (Bonaventure *et al.*, 2003; Salas and Ohlrogge, 2002). There are eight FatAs and two FatBs in *R. ovatum*, which is similar to the two rhododendrons (Figure S18). Of the five expressed FatAs, Ro_05316 and Ro_25510 had higher mRNA levels in leaves and stems compared with flowers, whereas Ro_05310, Ro_05307 and Ro_28441 were mainly expressed in flowers (Figure 4c). The two FatBs had similar expression in leaves and flowers, and the levels were considerably increased compared with that in stems.

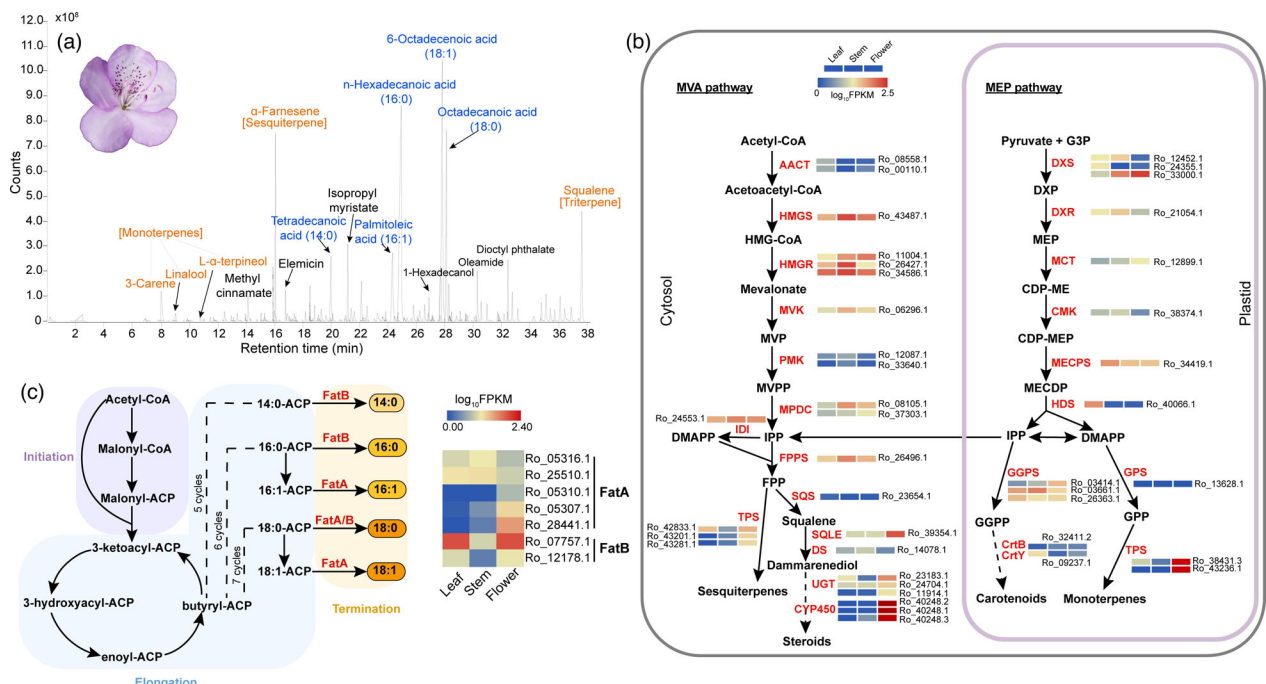


Figure 4 Flora volatiles compounds and biosynthesis pathways. (a) Gas chromatogram of floral volatiles from the flower of *R. ovatum*. Compounds shown in orange are terpenes and that in blue are fatty acids. (b) Expression profiles of genes encoding enzymes involved in canonical terpenoid biosynthesis pathways. Abbreviations for enzymes in each catalytic step are shown in red and their full names are listed in Data S3. (c) The fatty acid biosynthesis pathway and expression profiles of the genes coding the key enzymes FatA and FatB in leaf, stem, and flower tissues.

TPSs evolution reveals loss of flora fragrance in the other *Rhododendron* species

The terpene products of TPSs are extremely diverse and constitute the largest class of plant secondary metabolites (Dudareva *et al.*, 2005). Besides their role in floral scents biosynthesis and plant response to abiotic environmental stress, such as heat stress previously mentioned, terpenes are involved in plant defences against various biotic stresses (Pichersky and Gershenzon, 2002). In addition, terpenes may function as chemical signals mediating beneficial interactions between plants and other organisms (Pichersky and Gershenzon, 2002). Therefore, the TPS family plays an important role in plant adaptation. One of the most striking features of the *R. ovatum* genome is the extremely expanded large number of TPS genes (*RoTPS*). There are 111 *RoTPS* genes in *R. ovatum* genome (Figure S19 and Data S4), which is significantly larger than that of other *Rhododendron* species [*R. simsii* (65), *R. delavayi* (49) and *R. williamsianum* (43)] without floral scents. Moreover, the TPS number of *R. ovatum* is also larger than *A. chinensis* (32), *C. sinensis* (72), *S. lycopersicum* (52), wintersweet (52) (Shang *et al.*, 2020) and most of the other plants (Chen *et al.*, 2011). Phylogenetic analyses of TPS from seven species showed that *RoTPS*s are ascribed to six previously recognized TPS subfamilies, TPS-a, TPS-b, TPS-c, TPS-e, TPS-f and TPS-g and showed 1–3 *Rhododendron*-specific clades within the TPS subfamilies (Figure 5a, Figures S20–S26). The majority of *RoTPS*s were classified into the TPS-a and TPS-b subfamilies (Figures S19 and S20). Comparative genomic analysis showed that *RoTPS*s have been extremely expanded, especially in the TPS-b subfamily (Figure 5a, Figures S19–S26). Chromosome localization showed that numerous *RoTPS* genes occur in tandem arrays especially on chromosomes 6 and 7, where 27 (TPS025–TPS051) and 16 (TPS055–TPS070) TPS genes are organized as extremely dense gene clusters across stretches of 921 and 378 kb, respectively (Figure S27 and Data S4).

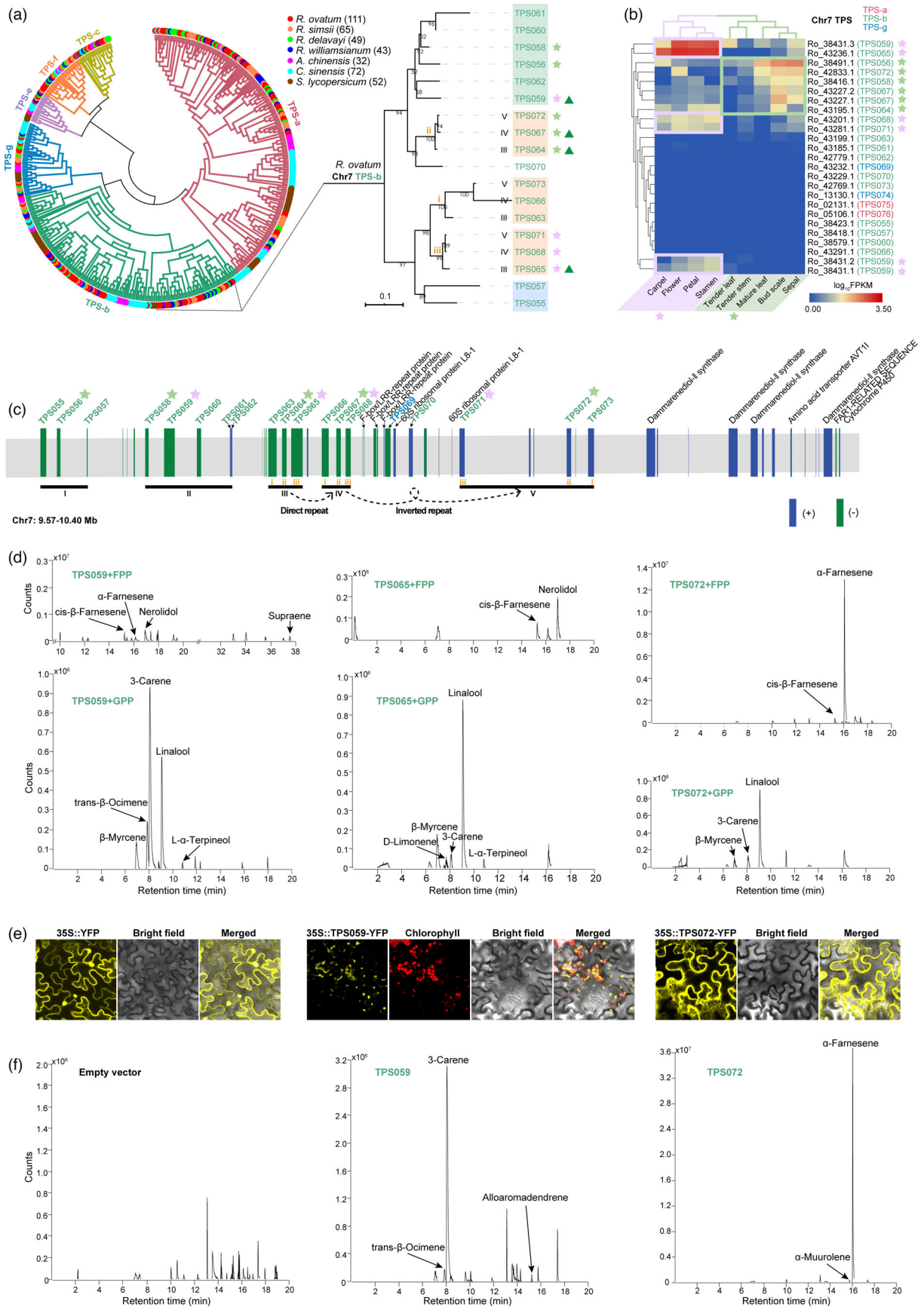
Expression analysis of the 111 *RoTPS* genes by RNA-seq of leaf, stem, bud scale and floral tissues (whole flower, petal, sepal, stamen and carpel) demonstrated that most of the genes had no or low expression, whereas the highly expressed genes had a concentrated distribution on chromosome 7 (Chr7) (Figure S28). Expression profiles of TPS genes in sepal were clustered with that in vegetative green tissues instead of other floral tissues (Figure 5b). There are eighteen TPS-b, two TPS-a and two TPS-g genes on Chr7, and only transcripts of TPS-b genes were expressed in the tissues, of which some were mainly expressed in the green tissues and some in flora tissues. Among the TPS transcripts, Ro_38431.3 (*TPS059*) and Ro_43236.1 (*TPS065*) exhibited high abundance in floral tissues. The other two alternative splicing transcripts (Ro_38431.1 and Ro_38431.2) of *TPS059* exhibited much lower expression levels than Ro_38431.3.

Sequence alignment of the three transcripts of *TPS059* to genomic DNA showed that Ro_38431.3 lacks an exon that encodes 32 and 22 amino acids for Ro_38431.1 and Ro_38431.2, respectively (Figure S29). The TPS-b of Chr7 were clustered into two major clades in phylogenetic analysis, and only four TPSs (*TPS059*, 064, 065 and 067) contain predicted plastid transit peptides, indicating that other expressed TPS-b proteins (*TPS058*, 056, 071, 068 and 072) probably work in the cytosol (Figure 5a, Figure S30).

The TPS gene clusters located within the 9.57–10.40 Mb region on Chr7 showed more detailed relationships among these genes (Figure 5c). According to the tandem repeat identification, there are five tandem repeat modules (I–V) of the 17 TPS genes with 4 on the plus strand and 13 on the minus strand. *TPS055* and *TPS057* of module I are sister gene pairs, while *TPS056* are in the clade of module II genes (Figure 5a), which indicates that *TPS056* and *TPS058* may result from a duplication event because of their close relationship and similar expression patterns. TPS genes of module III–V are evenly clustered to three phylogenetic clades (i, ii and iii) with the same gene relationships of the three modules. In combination with the phylogenetic relationship, chromosome location and gene expression profiles, we inferred that module IV duplicated from module III by direct repeat, and module V duplicated from module IV by inverted repeat. The differences in gene structure and expression profiles between the duplicated gene pairs, such as *TPS058* and *TPS059*, *TPS065* and *TPS068*, demonstrate that one of the gene copies may have occurred neofunctionalization. The adjacent genes of the TPS tandem arrays on Chr7 encoding F-box/LRR-repeat proteins, 60S ribosomal proteins L8-1 and Dammarenediol-II synthases also show the characteristic of tandem repeat, but they had very low or no expression in the samples detected with the exception of one *L8-1* gene (Figure S31). This finding reveals high transcriptional activity for TPSs and low transcriptional activity for the TPS-adjacent genes in the TPS densely distributed region on Chr7.

To validate whether the representative TPSs that have high expressions are crucial for flower cent biosynthesis, enzyme activities of recombinant *TPS059*, 065 and 072 were performed in vitro. The three TPSs can catalyse biosynthesis of sesquiterpenes (cis- β -farnesene, α -farnesene and nerolidol) and triterpene (supraene) when with FPP as substrate and of monoterpenes (β -myrcene, trans- β -ocimene, 3-carene, linalool and L- α -terpineol) when with GPP as substrate (Figure 5d). The subcellular localization showed that *TPS059* distributes in plastid and *TPS072* in the cytosol (Figure 5e). The in vivo expression of *TPS059* in tobacco leaves exhibited the main product of 3-carene, as well as little trans- β -ocimene and alloaromadendrene, and *TPS072* catalysed the main product of α -farnesene and little α -Muurolene (Figure 5f). These results demonstrate that the representative TPSs are crucial for flower cent biosynthesis in *R. ovatum*.

Figure 5 Characterization of terpene synthase-encoding genes in the *R. ovatum* genome. (a) Phylogeny of TPSs identified in *R. ovatum* and 6 other sequenced plant genomes. The numbers after species names indicate TPS gene numbers. Right panel shows details of the TPS-b clade on Chromosome 7 (Chr7) of *R. ovatum*. (b) Expression profiles of the TPS transcripts on Chr7. (c) Arrangement and chromosomal position as indicated of the 830-kb TPS gene cluster and adjacent genes on Chr7. The black lines under the genes indicate tandem repeat modules (I–V). The gene order of the genes in modules III–V are marked as i–iii. Stars indicate highly expressed genes, with purple indicating the members mainly expressed in flower tissues and green indicating that in vegetative tissues and sepal. Triangles indicate the genes that have plastid transit peptides coding sequence. (d) *In vitro* enzymatic products of recombinant TPS proteins incubated with farnesyl diphosphate (FPP)/geranyl diphosphate (GPP). (e) Subcellular localization of TPS-YFP fusion proteins in tobacco mesophyll cells. (f) *In vivo* enzymatic products of *TPS059* and 072 that transiently expressed in tobacco leaves. The volatile terpenes were analysed by GC-MS analysis.



To investigate whether floral fragrance was gained in *R. ovatum* after its divergence from other species or floral fragrance was lost in other *Rhododendron* species, the evolutionary history of TPS-b, the mainly expressed subfamily related to floral scents, was further analysed. Phylogenetic analyses of TPS-b from seven species showed that *Rhododendron* TPS-b members were ascribed to four groups (b1–4) (Figure 6a). Most of the *R. ovatum* TPS-b genes are distributed on chromosomes 2, 7 and 12 as tandem arrays (Figure 6b). The b1 (*TPS001* and *TPS002*, with their sister gene pairs *TPS007* and *TPS008*, respectively) and b3 groups (*TPS003*–*006*, with their sister gene pairs *TPS009*–*TPS012*, respectively) are mainly distributed on Chr2, and gene cluster *TPS009*–*TPS012* are likely duplicated from *TPS001*–*TPS006*. The b2 and b4 groups are mainly distributed on Chr12 and Chr7, respectively. Collinearity analysis of TPS-b-located regions between *R. ovatum* and *R. simsii* showed that many chromosomal variations (including insertion, deletion or translocation or inversion) as well as tandem duplication have occurred during their evolutionary history, which resulted in more TPS-b genes in *R. ovatum* than *R. simsii* (Figure 6b).

As the expressed TPS proteins all have more than 500 amino acids and complete motifs, we use this length to define the

relatively complete sequences. *R. ovatum* has 28 complete TPS-b sequences, which is much more than that in *R. simsii* (4), *R. williamsianum* (2) and *R. delavayi* (6) (Figure 6a). According to the phylogenetic relationship of TPS-b in four *Rhododendron* species, we identified and named orthologous members based on the TPS-b names of *R. ovatum* and aligned them with the species lineage phylogeny (Figure 6c). Four *Rhododendron* species all possess b1–4 groups of TPS-b subfamily, which indicated the existing of the four TPS-b groups in *Rhododendron* ancestor. However, *R. ovatum* has more members of each group compared with the other three species. For the highly expressed TPS genes in *R. ovatum*, the other three species have some of the orthologues, such as TPS056, 064, 065, 067 and 072, but only the orthologues that are highly expressed in vegetative tissues have complete sequences. *R. williamsianum* has the TPS065 orthologues that are highly expressed in *R. ovatum* floral tissues but with incomplete sequence (Rw 9456154.1). TPS065 of *R. ovatum* also generated two more copies (TPS068 and 071), and they all have high transcript levels in floral tissues, which may enhance the content or diversity of terpenes. Another highly expressed gene in *R. ovatum* floral tissues, TPS059, generated earlier than TPS064, 070, 055, 063, 065 and their copies of the

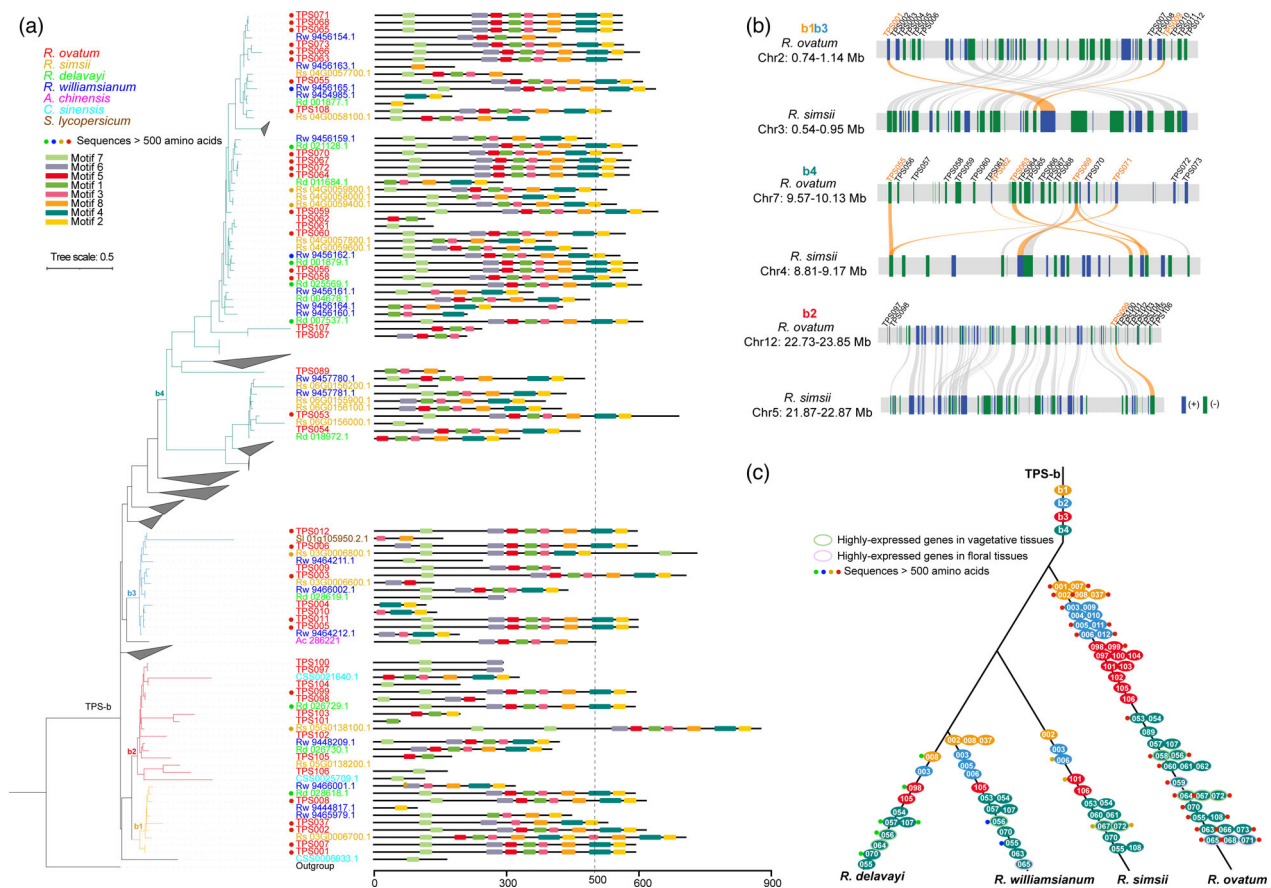


Figure 6 Evolution of TPS-b genes in *Rhododendron* species. (a) Phylogeny tree of TPS-b subfamily identified in *R. ovatum* and 6 other sequenced plant genomes. The b1–4 indicate four groups of *Rhododendron* TPS-b. Motifs were predicted using MEME tool (<http://meme-suite.org/tools/meme>). The length of 500 amino acids was used to define relatively complete sequences. (b) Intergenomic synteny blocks of the TPS-b-located chromosome regions of *R. ovatum* and *R. simsii*. TPS-b gene names of *R. ovatum* were marked above the gene blocks and the lines link the syntenic TPS-b genes are highlighted in orange. (c) Schematic drawing of the evolution history of TPS-b aligned with the lineage phylogeny of *R. ovatum*, *R. simsii*, *R. williamsianum*, and *R. delavayi*. The black lines indicate the lineage phylogeny of the four *Rhododendron* species. The TPS-b orthologues are aligned in the branches according to the phylogeny relationships. The complete sequences and the highly expressed genes in vegetative or floral tissues were marked.

other three species (Figure 6a) but still have high sequence similarity with them, which indicates that the other three species may have lost TPS059 orthologues. From these results, we inferred that the other three *Rhododendron* species likely lost floral fragrance in evolutionary history, which has tight relationships with the loss and fragmentation of the essential genes for floral scents biosynthesis.

Discussion

In this study, we present a high-quality reference genome assembly for the evergreen azalea species *R. ovatum*, which has important ornamental value and evolutionary position in the genus *Rhododendron*. The high heterozygosity of 1.55% presents a significant challenge for genome assembly. We applied PacBio sequencing technology and assembled the genome by Falcon using `purge_haplotigs` to filter redundant sequences from heterozygous genomic regions. The *R. ovatum* genome has a higher quality of assembly and annotation compared with other sequenced species in Ericales. Thus, the genome assembly of *R. ovatum* improved the quantity and quality of genome information not only for *Rhododendron* but also for Ericales. In addition, the genome analyses provide more evidence that the WGD of *Ad-β*, which was previously identified in the analysis of the kiwifruit genome (Huang et al., 2013; Shi et al., 2010; Tang et al., 2019; Wu et al., 2019), was shared by some families within Ericales (Zhang et al., 2020a). Importantly, phylogenetic analysis indicated that *R. ovatum* (subgenus *Azaleastrum*) diverged from *Rhododendron* ancestor earlier than *R. simsii* (subgenus *Tsutsusi*), *R. delavayi* and *R. williamsianum* (subgenus *Hymenanthes*). However, the genetic variance between *R. ovatum* and *Hymenanthes* is less than that between *R. simsii* and *Hymenanthes*, which explains why *Azaleastrum*, compared with *Tsutsusi*, has more similar morphological characteristics with *Hymenanthes*. Thus, the early but conservative evolution of *R. ovatum* probably makes it similar to the *Rhododendron* ancestor, and its genome will contribute to resolving the origin of *Rhododendron*.

Habitat heterogeneity was proved to have the highest effects on species diversity and net diversification rate in the genus *Rhododendron* (Shrestha et al., 2018). The availability of the *R. ovatum* genome sequence facilitates in-depth comparative genomic analysis to elucidate the evolution and adaptation divergences between low-altitude azalea and high-altitude rhododendron. Numerous studies have reported cold and ultraviolet tolerance of alpine plants (Klatt et al., 2018; Larson et al., 1990; Peng et al., 2011; Zhang et al., 2019a, 2019b), but the adaptation advantages of low-altitude plants have rarely been investigated. It is commonly considered that high temperatures may be the primary factor of low-altitude environments compared to high altitudes (Wang et al., 2020; Zhang et al., 2019a). However, a comparison of *R. ovatum* with *R. delavayi* and *R. williamsianum* showed significant expansion of genes related to diverse biotic and abiotic responses, although high-temperature-responsive genes (*HSP70s* and *TPSs*) are also included. The enriched GO terms, such as response to nematode, nitrogen, water deprivation, hypoxia and acidic pH, provided probable evidence that points to the rhizosphere environment. These findings indicated that low-altitude azaleas have encountered more complex stresses in addition to higher temperatures compared to alpine rhododendrons. A species living in a specific environment has the tendency of preferential amplification of gene responses to environmental factors. The significantly

enriched expansive hormone signals in *R. ovatum* are SA and JA, which play important roles in various physiological processes, especially in biotic stress responses (Clarke et al., 2000; Kanno et al., 2012). This finding is consistent with the fact that more pathogens are present in low-altitude environments compared with high-altitude environments (Zhang et al., 2019a). The transcription factors MYB, ERF and NAC are important regulators in defence responses (Riechmann and Ratcliffe, 2000). One *ANAC001* subfamily member of the *NAC* family in *Chrysanthemum lavandulifolium* named *CINAC4* was induced by salt, drought, cold or ABA treatment (Huang et al., 2012). The expression of the *ANAC001* subfamily member of Chinese cabbage increased under both cold and heat stress (Ma et al., 2014). These reports imply that the significantly expanded *ANAC001* subfamily of *R. ovatum* may have important roles in abiotic stress responses. The expansive genes involved in the stress responses of *R. ovatum*, we expect, lie the unique solutions to understanding the particular adaptation to its low-altitude ecological niche.

Terpenoids are the largest class of secondary metabolites in plants (Dudareva et al., 2005). Terpenes can be released from vegetative and floral tissues to attract pollinators or protect plants by attracting predators of attacking herbivores, and they can also serve directly as toxic agents against herbivores or pathogens (Gershenzon and Kreis, 1999; Pichersky and Gershenzon, 2002). Regarding the terpenes in flower VOCs of *R. ovatum*, three monoterpenes, one sesquiterpene and one triterpene were detected, demonstrating significant diversity in functions. Among the terpenes in *R. ovatum*, a sesquiterpene (α -farnesene) exhibited the highest content. In general, sesquiterpene synthases belong to the TPS-a group (Chen et al., 2011). However, farnesene synthase has been reported to be coded by TPS-b members in apple (Green et al., 2007) and soybean (Lin et al., 2017). (E)- β -farnesene was detected in floral VOCs of water lily but no gene was found in the TPS-a clade, and a member of TPS-b, which is highly expressed in flowers, was deduced to be a candidate gene for sesquiterpene synthase (Zhang et al., 2020b). Moreover, two tandem-duplicated TPS-b genes *TPS02* and *TPS03* showed (E)- β -ocimene and (E,E)- α -farnesene synthase activities in two ecotypes of Arabidopsis, respectively, and their differential subcellular compartmentalization in plastids and the cytosol was responsible for the ecotype-specific difference (Huang et al., 2010). In addition, it was also found that sesquiterpenes could be catalysed by TPS-e (Sallaud et al., 2009) or TPS-g (Aharoni et al., 2004). Overall, in recent years, numerous studies have demonstrated that plants have evolved complex routes for terpene biosynthesis, including new enzymes, alternative substrates and localization (Sun et al., 2016). Hence, the functions or species specificity of TPS may be more complex than previously thought. In the present study, the *in vitro* enzyme activities showed that TPSs can use both FPP and GPP as substrate to synthesize sesquiterpene and monoterpene, respectively. However, the *in vivo* enzyme activities showed that plastid-localized TPS059 mainly catalyse monoterpene synthesis while cytosol-localized TPS072 mainly catalyse sesquiterpene synthesis. Therefore, our study demonstrated that differential subcellular compartmentalization is the dominant factor for TPSs function, like in above-mentioned Arabidopsis (Huang et al., 2010). *TPS-b* genes without plastid transit peptide coding sequences can participate in sesquiterpene synthesis in the cytosol. Moreover, TPS-b members expressed not only in flower but also vegetative tissue of *R. ovatum*, which indicates that they probably play major roles in floral fragrance as well as defence responses.

Flower colour and fragrance are equally important in terms of attracting consumers of ornamentals, and these two traits are essential for the attraction of pollinators and hence for the evolutionary success of plants (Parachnowitsch *et al.*, 2012; Zuker *et al.*, 2002). Large amounts of *Rhododendron* species have bright and beautiful flowers but no floral fragrance. It is common for the flowering plant that bright coloured flowers have no or less fragrance compared with light coloured flowers, which is a balance for pay (energy distribution on flower colour or fragrance) and gain (attraction of pollinators). The carnation plants with colour modification resulted in lighter colour and more fragrant than control plants, which was due to diversion of metabolic flow from anthocyanin biosynthesis for colour to benzoic acid production for fragrance, both originating from the phenylpropanoid pathway (Zuker *et al.*, 2002). Moreover, the anthocyanin biosynthetic enzyme chalcone isomerase could modulate terpenoid production in glandular trichomes of tomato, although the mechanisms were not clarified (Kang *et al.*, 2014). There may be complementary relationships between flower colour and fragrance of *Rhododendron* plants, as *R. simsii* and *R. delavayi* have bright red flowers without fragrance, whereas *R. ovatum* has light pinkish purple flowers with delightful aroma, and some white flowers generally exhibit strong fragrance (Cameron, 1993). The less *TPS* genes of other *Rhododendron* species may be related to the loss of floral fragrance, and the expansion of the *TPS* genes in *R. ovatum* not only promotes the retention of the floral fragrance but also is related to the greater diversity of the floral fragrant compounds.

An important type of duplication common in genome is tandem duplication, where identical copies appear next to each other (Hanada *et al.*, 2008). The tandem duplication occurred not only from single gene but also from gene clusters with mode of direct repeat or inverted repeat. In addition, the gene retention following tandem duplication shows a bias in comparison to segmental and whole-genome duplication and often exhibits a lineage-specific fashion (Freeling, 2009), which can be confirmed in the subfamilies a and b of *TPS* and ANAC001 of NAC in present study. The characteristics of tandem duplication of *TPS* genes are commonly found in other plants (Chaw *et al.*, 2019; Shang *et al.*, 2020; Xia *et al.*, 2020). However, in this study, tandem duplication has more contribution to the diversification of *TPS* genes associated with the production of terpenoids for floral scents and defence responses of *R. ovatum* compared with the other *Rhododendron* species. In a previous report, the genes responsive to abiotic or biotic stimuli were most multiplied by tandem duplication in the comparison of the extremophile crucifer *Thellungiella parvula* with *Arabidopsis thaliana* (Dasanayake *et al.*, 2011). Other studies also supported the notion that expanded genes via tandem duplication tend to be involved in responses to various stresses, which is important for adaptive evolution to dynamically changing environments (Hanada *et al.*, 2008; Myburg *et al.*, 2014). Our analyses of tandem-duplicated genes showed that most of these genes contain stress-related domains and are involved in defence-responsive biological processes. The GO enrichments for tandem-duplicated genes and the expansive genes of *R. ovatum* compared with the high-altitude rhododendrons exhibited high similarity, which indicates that tandem duplication has tight relationships with the genes mediating extensive adaptability of *R. ovatum* in the complex environments of low-altitude areas. Despite the same genus undergoing same WGD events, azaleas and rhododendrons have different habitat preferences, which are probably due to the

subsequent high rate of tandem duplications of stress-responsive genes. Therefore, tandem duplication is the primary evolutionary force driving the expansion of genes related to stress responses, especially for the divergent evolution of the closely related species that experienced the same WGD events.

In conclusion, we report a high-quality chromosome-level reference genome of the evergreen azalea *R. ovatum* and provide novel insights into tandem duplication-facilitated low-altitude adaptation and flower fragrance. We identified the biological processes and candidate genes associated with biotic and abiotic stress responses, which can be taken into consideration in domestication and breeding of alpine rhododendrons for urban landscaping. In addition, the genome sequence will provide valuable resources for evolutionary research of *Rhododendron* and Ericales.

Materials and methods

Plant materials and sequencing

An individual plant of *R. ovatum* growing at the Ornamental Germplasm Resource Nursery of Zhejiang University, Hangzhou, China, was used for reference genome construction. *R. ovatum* is an azalea species with several excellent ornamental traits, such as evergreen features, graceful architecture, elegant and fragrant flowers, and resistance to complex environmental stresses. Fresh tissues, including mature leaves, tender leaves, tender stems, bud scale, whole flower and different tissues of flower (sepal, petal, stamen and carpel), were harvested and immediately frozen in liquid nitrogen. Samples were stored at -80°C prior to DNA or RNA extraction.

High-quality genomic DNA was extracted from the tender leaves of *R. ovatum* using a modified CTAB method (Porebski *et al.*, 1997). Approximately 20-kb SMRTbell libraries were constructed for PacBio sequencing on the PacBio Sequel platform. Hi-C libraries were also constructed from tender leaves and sequenced using the MGISEQ-2000 system. Samples collected from three tissues (leaves, stems and flowers) were used to construct individual SMRTbell libraries, and the libraries were pooled with equimolar ratios before ISO-seq. All of the raw sequencing data were filtered using SOAPnuke (v 1.6.5) (Chen *et al.*, 2018) to remove the reads that exhibit low quality, adapter contamination and PCR duplication before subsequent analyses.

Genome assembly and quality assessment

Genome size and heterozygosity were evaluated by *k*-mer analysis using Illumina sequence data. The long reads generated from PacBio sequencing were initially assembled into contigs using Falcon/Falcon-Unzip with parameters 'length_cutoff = -1, seed_coverage = 40' (PacBio Assembly Tool Suite) (<https://github.com/PacificBiosciences/pb-assembly>) (Chin *et al.*, 2016), and the contigs were self-corrected using Arrow (<https://github.com/PacificBiosciences/GenomicConsensus>). The resultant sequences from heterozygous regions were then removed using purge_haplotigs (Roach *et al.*, 2018) (https://bitbucket.org/mroac/hawri/purge_haplotigs) with parameters '-a 75 -m 500'. To increase the accuracy of the assembly, the short reads used in the genome survey were recruited for further polishing with the Pilon program (v1.23) (<https://github.com/broadinstitute/pilon>). The paired-end reads from Hi-C were used to cluster, order and orient the draft contigs onto chromosomes using the ALLHiC (v 0.8.11) pipeline (<https://github.com/tangerzhang/ALLHiC>) (Zhang *et al.*, 2019b).

Two assessment strategies, BUSCO alignment and transcript alignment, were performed to evaluate the assembly quality of the *R. ovatum* genome. The Eudicotyledons_odb10 dataset (busco.ezlab.org) was employed to evaluate the completeness of the genome assembly using BUSCO (v 3.1.0) (Simao *et al.*, 2015). The polished transcripts generated from PacBio ISO-seq were aligned to the genome assembly using Minimap2 (v 2.6) (Li, 2018) to assess the accuracy of the *R. ovatum* genome. We evaluated the assembly continuity by calculating the LAI score with LTR-RTs using LTR_retriever (v 2.6) (https://github.com/oushujun/LTR_retriever) (Ou and Jiang, 2018).

Gene prediction and functional annotation

De novo and homologous predictions were integrated to identify repetitive sequences. LTR_Finder (v 1.07) (parameters: -D 15000 -d 1000 -L 7000 -l 100 -p 20 -C -M 0.9) and LTRharvest (GenomeTools suite v1.5.9) (parameters: -similar 90 -vic 10 -seed 20 -seqids yes -minlenltr 100 -maxlenltr 7000 -mintsd 4 -maxtsd 6 -motif TGCA -motifm 1) were first used to identify candidate LTR-RTs, and the outputs were feeded to LTR_retriever (https://github.com/oushujun/LTR_retriever) (Ou and Jiang, 2018) to generate non-redundant LTR-RT library. This library was used in *de novo* prediction to obtain LTR elements. Other repeats were identified using RepeatModeler (v 1.0.11) (<https://github.com/Dfam-consortium/RepeatModeler>) (Flynn *et al.*, 2020). The LTR elements and other repeats were merged to the *de novo* repeats database. Homologous predictions were performed using RepeatMasker (v 4.0.5) (<http://www.repeatmasker.org/>) (Tarailo-Graovac and Chen, 2009) based on the *de novo* repeats database, Repbase and TE protein database. Repetitive sequences in the *R. ovatum* genome were masked before gene prediction. The *ab initio* prediction was performed by using the BRAKER2 pipeline (v 2.1.5) (<https://github.com/Gaius-Augustus/BRAKER>) (Bruna *et al.*, 2021). In addition, GlimmerHMM and SNAP were used for *ab initio* gene predictions with gene model parameters trained from *R. delavayi* and *V. corymbosum*. We aligned the protein sequences from *R. delavayi*, *V. corymbosum*, *A. chinensis*, *P. vulgaris* and *C. sinensis* to the *R. ovatum* genome using GeMoMa (v 1.4.2) (<http://www.repeatmasker.org/>) (Keilwagen *et al.*, 2019) in homology predictions. For transcriptome-based predictions, the full-length transcripts obtained by PacBio sequencing were aligned to the assembled genome by PASA (<https://github.com/PASApipeline/PASApipeline>) (Haas *et al.*, 2008). Finally, all evidence from *ab initio*, homology-based and RNA-seq-based predictions were combined into the consensus gene sets using the EVIDENCEModeler (v1.1.1) (<http://evidence.modeler.github.io/>) (Haas *et al.*, 2008) and then optimized with PASA (Haas *et al.*, 2008) to obtain the integrated gene model.

Functional annotation of protein-coding genes was performed using BLASTP (E-value cut-off $1e^{-5}$) homologue search against the NCBI non-redundant (Nr) protein database (2020-7-10) and Swiss-Prot database (2020-8-12). InterProScan package (v5.29-68.0) was used to run the scanning algorithms from the InterPro database to perform a comprehensive annotation including TIGRFAM, Phobius, SignalP, SUPERFAMILY, PANTHER, Gene3D, ProSite, Coils, PRINTS, SMART, Pfam, PIRSF, TMHMM and GO. eggNOG-mapper (v1.0.3, <https://github.com/eggNOGdb/eggNOG-mapper>) was used for functional annotation based on fast orthology assignments using precomputed clusters and phylogenies from the eggNOG database. GO and KO (KEGG Orthology) information was retrieved from InterPro and eggNOG annotation. In addition, KAAS (KEGG Automatic Annotation Server) ([\[www.genome.jp/tools/kaas/\]\(http://www.genome.jp/tools/kaas/\)\) was used to provide functional annotation of genes by BLAST against the KEGG GENES database to obtain KO assignments and automatically generated KEGG pathways.](https://</p>
</div>
<div data-bbox=)

Construction of species phylogenetic tree

Protein sequences of *R. ovatum*, *R. simsii*, *R. delavayi*, *R. williamsianum*, *Actinidia chinensis*, *Camellia sinensis*, *Diospyros lotus*, *Primula vulgaris* and *Solanum lycopersicum* were collected for the construction of the species phylogenetic tree. Orthofinder (v 2.4.0) (Emms and Kelly, 2015), an integrated tool for gene family clustering, was adopted for the analysis of gene families. The protein datasets for the chosen species were clustered into orthologous groups and paralogous groups at first, and then, genes of single-copy orthologous groups were selected for the alignment and construction of the species phylogenetic tree. After the single-copy orthologues were obtained, the longest protein sequences of each single-copy gene were extracted according to the Orthofinder results. ClustalO (v 1.2.4) (Madeira *et al.*, 2019) was used for the multiple sequence alignment (MSA) of protein sequences, and then trimAl (v 1.2.rev59) (Capella-Gutierrez *et al.*, 2009) was adopted for the trimming of MSA results. We chose RAXML (v 8.2.12) (Stamatakis, 2014) finally for the construction of a species tree exhibiting the phylogenetic relationship of selected species using trimmed MSA results with the concatenation method.

Divergence time estimation and gene family expansion

After construction of the species phylogenetic tree, the calibration time of divergence of these species was obtained from TimeTree (<http://www.timetree.org/>) (Hedges *et al.*, 2015), a database for calibration time among different species supported by integrated studies, as the benchmark of the following analysis. Single-copy orthologous genes are required for the analysis of fourfold degenerate sites. We applied MCMCTree, a tool comprised in the PAML software package (Yang, 2007), for the construction of the ultrametric tree, which contains not only phylogenetic relationships but also 95% confidence intervals of divergence time. The CAFE (v 4.2.1) (Han *et al.*, 2013) workflow with a probabilistic graphical model was then chosen for the analysis of gene family expansion and contraction with *P*-value of 0.05.

Polyploidization events analysis

The longest protein sequences of each gene within the genomes of *R. ovatum*, *A. chinensis*, *C. sinensis*, *D. lotus*, *R. delavayi*, *R. williamsianum*, *S. lycopersicum* and *V. vinifera* were selected for synteny and collinearity detection within themselves using mcscan, a tool contained in JCVI (Goll *et al.*, 2010), to shed light on polyploidization events. PAML (v 4.9i) (Yang, 2007) was chosen to compute the *Ks* value between gene pairs of synteny gene blocks. For *R. ovatum*, we modelled the distribution of *Ks* rates as a mixture model and identified syntenic gene pairs falling within the *Ks* ± 1 SD as paralogs likely derived from the *Ad-β* and *At-γ* event (Teh *et al.*, 2017). *Ks* Dot plots of orthologues between genomes and intergenomic synteny blocks were visualized using TBtools (v 1.074) (Chen *et al.*, 2020). Types of gene duplication and tandem repeats were analysed using MCScanX (Wang *et al.*, 2012) and TBtools (v 1.045) (Chen *et al.*, 2020).

RNA sequencing and gene expression analysis

All tissue samples mentioned above and leaves with different temperature treatments (25, 37 and 42 °C) were used to perform

RNA sequencing on the Illumina nova-seq 6000 platform. After obtaining reads data of transcriptomes, Trimmomatic (v 0.39) (Bolger *et al.*, 2014) was used for the trimming of the adapter sequences. Then, HISAT2 (v 2.2.1) (Wen, 2017) was chosen for the mapping of trimmed sequences to genome assemblies, followed by the analysis for FPKM (Fragments Per Kilobase per Million) using StringTie (v 2.1.4) (Pertea *et al.*, 2015). Gene co-expression networks were analysed by weighted correlation network analysis (WGCNA) (Langfelder and Horvath, 2008) and visualized by using Cytoscape (v 3.8.0) (Smoot *et al.*, 2011). Gene expression profiles of different tissues were presented as heatmaps using TBtools (v 1.045) (Chen *et al.*, 2020).

Determination of floral volatiles by GC-MS analysis

The floral volatiles of *R. ovatum* were detected using a headspace solid-phase microextraction system combined with gas chromatography–mass spectrometry (GC–MS). One gram of fully opened flower petals (approximately five flowers) was detached and immediately put into sample vials, and the volatiles were extracted with solid-phase microextraction (SPME, Supelco) for 30 min in a water bath at 50 °C. Then, the SPME was immediately transferred to the injection port (250 °C) of the GC-MS system (Agilent 7890B-7000C) to be desorbed for 5 min. Separation was performed on an HP-5MS capillary column (30 m × 0.25 mm) with helium as the carrier at a flow rate of 1 mL/min under splitless injection conditions. The temperature programming started from an initial oven temperature at 50 °C (2-min hold) and a temperature gradient of 5 °C per min increase to 180 °C (5-min hold) followed by a temperature gradient of 10 °C per min increase to 250 °C (8-min hold). Other settings included electron impact ionization (EI) at 70 eV, a 230 °C ion source temperature, and a 280 °C interface temperature. The mass spectrum was analysed in the range of 20–350 atom mass units. National Institute of Standards and Technology mass spectral database (NIST17.L) was used to identify the mass spectra of the compounds.

Enzyme activities and subcellular localization of TPSs

For *in vitro* enzyme activity characterization, coding sequences of TPS059, 065 and 072 were amplified from cDNA of flower tissue of *R. ovatum* and cloned into the prokaryotic expression vector pCold TF containing a His tag and expressed in the *Escherichia coli* strain Rosetta (DE3). The recombinant His-TPSs proteins were induced by 0.3mM IPTG at 16 °C overnight and purified using the ProteinIso® Ni-NTA Resin (Transgen, Beijing, China) according to the manufacturer's instructions. Assays for TPS enzyme activity were performed in a 1 mL assay buffer (30 mM HEPES, pH 7.5, 5 mM DTT, 25 mM MgCl₂) containing 10 µg purified TPS proteins and 60 µM GPP/FPP (Shang *et al.*, 2020). The mixture was incubated at 30 °C for 1 h and then 45 °C for 15 min before the synthesized volatiles were collected and analysed using the same methods with flower scents measurement.

For subcellular localization and enzyme activity characterization, coding sequences of TPS059 and 072 were cloned into pHB vector to obtain constructs of 35S::TPSs-YFP. Then, the plasmids were transformed into *Agrobacterium tumefaciens* strain GV3101 and injected into tobacco (*Nicotiana benthamiana*) leaves. After 2 days of incubation, the injected parts were sampled for subcellular localization observation by laser scanning confocal microscope and for volatile detection by headspace solid-phase microextraction with GC-MS.

Gene family identification and characterization

HMM search (Finn *et al.*, 2011) and BLASTp (Altschul *et al.*, 1990) were integrated to identify gene family members. The predicted proteins of the *R. ovatum* genome were screened by HMM search (Finn *et al.*, 2011) with Pfam motifs (<http://pfam.xfam.org>) of the target gene family. The hits with E-values greater than 1e-5 were individually evaluated. In addition, gene homologs were obtained by running a local BLASTp search (Altschul *et al.*, 1990) using previously characterized proteins from Swiss-Prot as queries against all protein sequences with an E-value cut-off of 1e-5. The obtained sequences from the two methods were integrated and manually checked to correct erroneous automatic annotation. Multiple sequence alignment was performed by MAFFT (v 7.467) (Katoh and Standley, 2013) with default parameters, and the maximum likelihood tree was constructed using FastTree (v 2.1.11) (Price *et al.*, 2009). Tree visualization and labelling were performed on MAGA (v 7.0.26) (Kumar *et al.*, 2016) or iTOL (<https://itol.embl.de/>) (Letunic and Bork, 2019). Plastid transit peptide was predicted using ChloroP 1.1 Server (Emanuelsson *et al.*, 1999). Chromosome localization and gene structure were visualized using TBtools (v 1.045) (Chen *et al.*, 2020).

Tandem duplication analysis

The genes generated by tandem duplication were identified using MCScanX (Wang *et al.*, 2012) inserted in TBtools (v 1.045) (Chen *et al.*, 2020). Tandem duplication ratio was calculated as number of genes generated by tandem duplication/total number of genes. Pfam domains were annotated using HMMER (v 3.1b2) (<http://hmmer.org/>) (Finn *et al.*, 2011) search against Pfam database (<http://pfam.xfam.org/>). The file of GO annotation for network analysis was prepared using TBtools (v 1.045) (Chen *et al.*, 2020) and visualized using BiNGO in Cytoscape (v 3.8.0) (Smoot *et al.*, 2011).

Acknowledgements

This work was supported by the National Natural Science Foundation of China (grant number 31901356 and 31800597), the Fundamental Research Funds for the Central Universities (grant number 2021QNA6021), and Zhejiang Science and Technology Major Program on Agricultural New Variety Breeding (grant number 2016C02056-12).

Competing interests

The authors declare that they have no competing interests.

Author contributions

Y.X., L.Z., and C.Z. conceived, designed the research, and managed the project. X.Y.W., H.Z., Z.L., B.L., and J.W. contributed to sample preparation and sequencing. X.P.W. and Y.G. performed the assembly and annotation. X.Y.W. and Y.G. analysed data and wrote the manuscript. X.H.W. and D.L. worked on WGCNA analyses. Fei C., Feng C., X.P.W., C.Z., L.Z., and Y.X. revised the manuscript. All authors read and approved the manuscript.

Data availability statement

The raw data files of genome sequencing and RNA sequencing have been deposited at Sequence Read Archive (SRA) under the

accession PRJNA671625. This whole-genome project also has been deposited at DDBJ/ENA/GenBank under the accession JADHZH000000000. Genome assembly and gene annotations could be downloaded from Rhododendron Plant Genome Database (http://bioinfor.kib.ac.cn/RPGD/download_genome.html).

References

- Aharoni, A., Giri, A.P., Verstappen, F.W.A., Berteaux, C.M., Sevenier, R., Sun, Z. K., Jongma, M.A. *et al.* (2004) Gain and loss of fruit flavor compounds produced by wild and cultivated strawberry species. *Plant Cell*, **16**, 3110–3131.
- Akagi, T., Shirasawa, K., Nagasaki, H., Hirakawa, H., Tao, R., Comai, L. and Henry, I.M. (2020) The persimmon genome reveals clues to the evolution of a lineage-specific sex determination system in plants. *Plos Genet.* **16**, e1008566.
- Altschul, S.F., Gish, W., Miller, W., Myers, E.W. and Lipman, D.J. (1990) Basic local alignment search tool. *J. Mol. Biol.* **215**, 403–410.
- Badouin, H., Gouzy, J., Grassa, C.J., Murat, F., Staton, S.E., Cottret, L., Lelandais-Briere, C. *et al.* (2017) The sunflower genome provides insights into oil metabolism, flowering and Asterid evolution. *Nature*, **546**, 148–152.
- Bolger, A.M., Lohse, M. and Usadel, B. (2014) Trimmomatic: a flexible trimmer for Illumina sequence data. *Bioinformatics*, **30**, 2114–2120.
- Bonaventure, G., Salas, J.J., Pollard, M.R. and Ohlrogge, J.B. (2003) Disruption of the FATB gene in Arabidopsis demonstrates an essential role of saturated fatty acids in plant growth. *Plant Cell*, **15**, 1020–1033.
- Bruna, T., Hoff, K., Lomsadze, A., Stanke, M. and Borodovsky, M. (2021) BRAKER2: automatic eukaryotic genome annotation with GeneMark-EP+ and AUGUSTUS supported by a protein database. *NAR Genomics Bioinform.* **3**, lqaa108.
- Burger, B.V., Munro, Z.M. and Visser, J.H. (1988) Determination of plant volatiles.1. Analysis of the insect-attracting allomone of the parasitic plant *Hydnora-africana* using grob-habich activated-charcoal traps. *J. High Resolut. Chromatogr. Chromatogr. Commun.* **11**, 496–499.
- Cameron, P. (1993) Fragrance in *Rhododendron* species. *J. Am. Rhodo. Soc.* **47**, 128–130.
- Capella-Gutierrez, S., Silla-Martinez, J.M. and Gabaldon, T. (2009) TrimAl: a tool for automated alignment trimming in large-scale phylogenetic analyses. *Bioinformatics*, **25**, 1972–1973.
- Chamberlain, D.F., Hyam, G., Argent, G., Fairweather, G. and Walter, K. (1996) *The Genus Rhododendron: Its Classification and Synonymy*. Edinburgh: Royal Botanical Garden.
- Chaw, S.M., Liu, Y.C., Wu, Y.W., Wang, H.Y., Lin, C.Y.I., Wu, C.S., Ke, H.M. *et al.* (2019) Stout camphor tree genome fills gaps in understanding of flowering plant genome evolution. *Nat. Plants*, **5**, 63–73.
- Chen, C.J., Chen, H., Zhang, Y., Thomas, H.R., Frank, M.H., He, Y.H. and Xia, R. (2020) TBtools: an integrative toolkit developed for interactive analyses of big biological data. *Mol. Plant*, **13**, 1194–1202.
- Chen, F., Tholl, D., Bohlmann, J. and Pichersky, E. (2011) The family of terpene synthases in plants: a mid-size family of genes for specialized metabolism that is highly diversified throughout the kingdom. *Plant J.* **66**, 212–229.
- Chen, Y., Chen, Y., Shi, C., Huang, Z., Zhang, Y., Li, S., Li, Y. *et al.* (2018) SOAPnuke: a MapReduce acceleration-supported software for integrated quality control and preprocessing of high-throughput sequencing data. *Gigascience*, **7**, 1–6.
- Chin, C.S., Peluso, P., Sedlazeck, F.J., Nattestad, M., Concepcion, G.T., Clum, A., Dunn, C. *et al.* (2016) Phased diploid genome assembly with single-molecule real-time sequencing. *Nat. Methods*, **13**, 1050–1054.
- Clarke, J.D., Volko, S.M., Ledford, H., Ausubel, F.M. and Dong, X.N. (2000) Roles of salicylic acid, jasmonic acid, and ethylene in cpr-induced resistance in Arabidopsis. *Plant Cell*, **12**, 2175–2190.
- Cocker, J.M., Wright, J., Li, J.H., Swarbrick, D., Dyer, S., Caccamo, M. and Gilmartin, P.M. (2018) *Primula vulgaris* (primrose) genome assembly, annotation and gene expression, with comparative genomics on the heterostyly supergene. *Sci. Rep.* **8**, 17942.
- Colle, M., Leisner, C.P., Wai, C.M., Ou, S., Bird, K.A., Wang, J., Wisecaver, J.H. *et al.* (2019) Haplotype-phased genome and evolution of phytonutrient pathways of tetraploid blueberry. *Gigascience*, **8**, 1–15.
- Dassanayake, M., Oh, D.H., Haas, J.S., Hernandez, A., Hong, H., Ali, S., Yun, D. J. *et al.* (2011) The genome of the extremophile crucifer *Thellungiella parvula*. *Nat. Genet.* **43**, 913–918.
- De Riek, J., De Keyser, E., Calsyn, E., Eeckhaut, T., Van Huylenbroeck, J. and Kobayashi, N. (2018) Azalea. In *Ornamental Crops*, (Van Huylenbroeck, J., ed.), pp. 237–271. Switzerland: Springer.
- Dudareva, N., Andersson, S., Orlova, I., Gatto, N., Reichelt, M., Rhodes, D., Boland, W. *et al.* (2005) The nonmevalonate pathway supports both monoterpene and sesquiterpene formation in snapdragon flowers. *Proc. Natl. Acad. Sci. USA*, **102**, 933–938.
- Emanuelsson, O., Nielsen, H. and Heijne, G.V. (1999) ChloroP, a neural network-based method for predicting chloroplast transit peptides and their cleavage sites. *Protein Sci.* **8**, 978–984.
- Emms, D.M. and Kelly, S. (2015) OrthoFinder: solving fundamental biases in whole genome comparisons dramatically improves orthogroup inference accuracy. *Genome Biol.* **16**, 157.
- Finn, R.D., Clements, J. and Eddy, S.R. (2011) HMMER web server: interactive sequence similarity searching. *Nucleic Acids Res.* **39**, W29–W37.
- Flynn, J.M., Hubley, R., Goubert, C., Rosen, J., Clark, A.G., Feschotte, C. and Smit, A.F. (2020) RepeatModeler2 for automated genomic discovery of transposable element families. *Proc. Natl. Acad. Sci. USA*, **117**, 9451–9457.
- Freeling, M. (2009) Bias in plant gene content following different sorts of duplication: tandem, whole-genome, segmental, or by transposition. *Annu. Rev. Plant Biol.* **60**, 433–453.
- Gershenzon, J. and Kreis, W. (1999) Biochemistry of terpenoids: monoterpenes, sesquiterpenes, diterpenes, sterols, cardiac glycosides and steroid saponins. In *Biochemistry of Plant Secondary Metabolism*, (Wink, M., ed.), pp. 222–299. Sheffield: Sheffield Academic Press.
- Goll, J., Rusch, D.B., Tanenbaum, D.M., Thiagarajan, M., Li, K., Methe, B.A. and Yoosheph, S. (2010) METARep: JCVI metagenomics reports an open source tool for high-performance comparative metagenomics. *Bioinformatics*, **26**, 2631–2632.
- Green, S., Friel, E.N., Match, A., Beuning, L.L., Cooney, J.M., Rowan, D.D. and MacRae, E. (2007) Unusual features of a recombinant apple alpha-farnesene synthase. *Phytochemistry*, **68**, 176–188.
- Haas, B.J., Salzberg, S.L., Zhu, W., Pertea, M., Allen, J.E., Orvis, J., White, O. *et al.* (2008) Automated eukaryotic gene structure annotation using EvidenceModeler and the Program to Assemble Spliced Alignments. *Genome Biol.* **9**, R7.
- Han, M.V., Thomas, G.W.C., Lugo-Martinez, J. and Hahn, M.W. (2013) Estimating gene gain and loss rates in the presence of error in genome assembly and annotation using CAFÉ 3. *Mol. Biol. Evol.* **30**, 1987–1997.
- Hanada, K., Zou, C., Lehti-Shiu, M.D., Shinozaki, K. and Shiu, S.H. (2008) Importance of lineage-specific expansion of plant tandem duplicates in the adaptive response to environmental stimuli. *Plant Physiol.* **148**, 993–1003.
- Hedges, S.B., Marin, J., Suleski, M., Paymer, M. and Kumar, S. (2015) Tree of life reveals clock-like speciation and diversification. *Mol. Biol. Evol.* **32**, 835–845.
- Huang, H., Wang, Y., Wang, S.L., Wu, X., Yang, K., Niu, Y.J. and Dai, S.L. (2012) Transcriptome-wide survey and expression analysis of stress-responsive NAC genes in *Chrysanthemum lavandulifolium*. *Plant Sci.* **193**, 18–27.
- Huang, M.S., Abel, C., Sohrabi, R., Petri, J., Haupt, I., Cosimano, J., Gershenzon, J. *et al.* (2010) Variation of herbivore-induced volatile terpenes among Arabidopsis Ecotypes depends on allelic differences and subcellular targeting of two terpene synthases, TPS02 and TPS03. *Plant Physiol.* **153**, 1293–1310.
- Huang, S.X., Ding, J., Deng, D.J., Tang, W., Sun, H.H., Liu, D.Y., Zhang, L. *et al.* (2013) Draft genome of the kiwifruit *Actinidia chinensis*. *Nat. Commun.* **4**, 2640.
- Jones, A., Davies, H.M. and Voelker, T.A. (1995) Palmitoyl-acyl carrier protein (ACP) thioesterase and the evolutionary origin of plant acyl-ACP thioesterases. *Plant Cell*, **7**, 359–371.
- Kang, J.H., McRoberts, J., Shi, F., Moreno, J.E., Jones, A.D. and Howe, G.A. (2014) The flavonoid biosynthetic enzyme chalcone isomerase modulates terpenoid production in glandular trichomes of tomato. *Plant Physiol.* **164**, 1161–1174.

- Kanno, H., Hasegawa, M. and Kodama, O. (2012) Accumulation of salicylic acid, jasmonic acid and phytoalexins in rice, *Oryza sativa*, infested by the white-backed planthopper, *Sogatella furcifera* (Hemiptera: Delphacidae). *Appl. Entomol. Zool.* **47**, 27–34.
- Katoh, K. and Standley, D.M. (2013) MAFFT multiple sequence alignment software version 7: improvements in performance and usability. *Mol. Biol. Evol.* **30**, 772–780.
- Keilwagen, J., Hartung, F. and Grau, J. (2019) GeMoMa: homology-based gene prediction utilizing intron position conservation and RNA-seq data. *Methods Mol. Biol.* **1962**, 161–177.
- Klatt, S., Schinkel, C.C.F., Kirchheimer, B., Dullinger, S. and Horandl, E. (2018) Effects of cold treatments on fitness and mode of reproduction in the diploid and polyploid alpine plant *Ranunculus kuepferi* (Ranunculaceae). *Ann. Bot.* **121**, 1287–1298.
- Knudsen, J.T., Eriksson, R., Gershenzon, J. and Stahl, B. (2006) Diversity and distribution of floral scent. *Bot. Rev.* **72**, 1–120.
- Knudsen, J.T., Tollsten, L. and Bergstrom, L.G. (1993) Floral scents—a checklist of volatile compounds isolated by head-space techniques. *Phytochemistry*, **33**, 253–280.
- Kobayashi, N., Mizuta, D., Nakatsuka, A. and Akabane, M. (2008) Attaining inter-subgeneric hybrids in fragrant azalea breeding and the inheritance of organelle DNA. *Euphytica*, **159**, 67–72.
- Kumar, S., Stecher, G. and Tamura, K. (2016) MEGA7: molecular evolutionary genetics analysis version 7.0 for bigger datasets. *Mol. Biol. Evol.* **33**, 1870–1874.
- Langfelder, P. and Horvath, S. (2008) WGCNA: an R package for weighted correlation network analysis. *BMC Bioinform.* **9**, 559.
- Larson, R.A., Garrison, W.J. and Carlson, R.W. (1990) Differential responses of alpine and non-alpine *Aquilegia* species to increased ultraviolet-B radiation. *Plant Cell Environ.* **13**, 983–987.
- Letunic, I. and Bork, P. (2019) Interactive tree of life (iTOL) v4: recent updates and new developments. *Nucleic Acids Res.* **47**, W256–W259.
- Li, H. (2018) Minimap2: pairwise alignment for nucleotide sequences. *Bioinformatics*, **34**, 3094–3100.
- Lin, J., Wang, D., Chen, X., Köllner, T.G., Mazarei, M., Guo, H., Pantalone, V.R. et al. (2017) An (E, E)- α -farnesene synthase gene of soybean has a role in defence against nematodes and is involved in synthesizing insect-induced volatiles. *Plant Biotech.* **15**, 510–519.
- Ma, J., Wang, F., Li, M.Y., Jiang, Q., Tan, G.F. and Xiong, A.S. (2014) Genome wide analysis of the NAC transcription factor family in Chinese cabbage to elucidate responses to temperature stress. *Sci. Hortic.* **165**, 82–90.
- Madeira, F., Park, Y.M., Lee, J., Buso, N., Gur, T., Madhusoodanan, N., Basutkar, P. et al. (2019) The EMBL-EBI search and sequence analysis tools APIs in 2019. *Nucleic Acids Res.* **47**, W636–W641.
- Ming, T.L. and Fang, R.Z. (1990) The phylogeny and evolution of genus *Rhododendron*. *Acta Bot. Yunnanica*, **12**, 353–365.
- Moriyama, Y. and Koshiha-Takeuchi, K. (2018) Significance of whole-genome duplications on the emergence of evolutionary novelties. *Brief. Funct. Genomics*, **17**, 329–338.
- Myburg, A.A., Grattapaglia, D., Tuskan, G.A., Hellsten, U., Hayes, R.D., Grimwood, J., Jenkins, J. et al. (2014) The genome of *Eucalyptus grandis*. *Nature*, **510**, 356–362.
- Norton, C.R. and Norton, M.E. (1989) *Rhododendrons*. In *Trees II* (Bajaj, Y.P.S., ed.), pp. 428–451. Berlin, Heidelberg: Springer Berlin Heidelberg.
- Ou, S. and Jiang, N. (2018) LTR_retriever: a highly accurate and sensitive program for identification of long terminal repeat retrotransposons. *Plant Physiol.* **176**, 1410–1422.
- Parachnowitsch, A.L., Raguso, R.A. and Kessler, A. (2012) Phenotypic selection to increase floral scent emission, but not flower size or colour in bee-pollinated *Penstemon digitalis*. *New Phytol.* **195**, 667–675.
- Peng, Y., Yang, Z.H., Zhang, H., Cui, C.Y., Qi, X.B., Luo, X.J., Tao, X.A. et al. (2011) Genetic variations in Tibetan populations and high-altitude adaptation at the Himalayas. *Mol. Biol. Evol.* **28**, 1075–1081.
- Pertea, M., Pertea, G.M., Antonescu, C.M., Chang, T.C., Mendell, J.T. and Salzberg, S.L. (2015) StringTie enables improved reconstruction of a transcriptome from RNA-seq reads. *Nat. Biotechnol.* **33**, 290–295.
- Pichersky, E. and Gershenzon, J. (2002) The formation and function of plant volatiles: perfumes for pollinator attraction and defense. *Curr. Opin. Plant Biol.* **5**, 237–243.
- Porebski, S., Bailey, L.G. and Baum, B.R. (1997) Modification of a CTAB DNA extraction protocol for plants containing high polysaccharide and polyphenol components. *Plant Mol. Biol. Rep.* **15**, 8–15.
- Price, M.N., Dehal, P.S. and Arkin, A.P. (2009) FastTree: computing large minimum evolution trees with profiles instead of a distance matrix. *Mol. Biol. Evol.* **26**, 1641–1650.
- Raguso, R.A. (2008) Wake up and smell the roses: The ecology and evolution of floral scent. *Annu. Rev. Ecol. Evol. Syst.* **39**, 549–569.
- Riechmann, J.L. and Ratcliffe, O.J. (2000) A genomic perspective on plant transcription factors. *Curr. Opin. Plant Biol.* **3**, 423–434.
- Roach, M.J., Schmidt, S.A. and Borneman, A.R. (2018) Purge Haplotigs: allelic contig reassignment for third-gen diploid genome assemblies. *BMC Bioinform.* **19**, 460.
- Salas, J.J. and Ohlrogge, J.B. (2002) Characterization of substrate specificity of plant FatA and FatB acyl-ACP thioesterases. *Arch. Biochem. Biophys.* **403**, 25–34.
- Sallaud, C., Rontein, D., Onillon, S., Jabes, F., Duffe, P., Giacalone, C., Thoraval, S. et al. (2009) A novel pathway for sesquiterpene biosynthesis from Z, Z-farnesyl pyrophosphate in the wild tomato *Solanum habrochaites*. *Plant Cell*, **21**, 301–317.
- Seki, H., Tamura, K. and Muranaka, T. (2015) P450s and UGTs: key players in the structural diversity of triterpenoid saponins. *Plant Cell Physiol.* **56**, 1463–1471.
- Shang, J.Z., Tian, J.P., Cheng, H.H., Yan, Q.M., Li, L., Jamal, A., Xu, Z.P. et al. (2020) The chromosome-level wintersweet (*Chimonanthus praecox*) genome provides insights into floral scent biosynthesis and flowering in winter. *Genome Biol.* **21**, 200.
- Shi, T., Huang, H.W. and Barker, M.S. (2010) Ancient genome duplications during the evolution of kiwifruit (Actinidia) and related Ericales. *Ann. Bot.* **106**, 497–504.
- Shrestha, N., Wang, Z.H., Su, X.Y., Xu, X.T., Lyu, L.S., Liu, Y.P., Dimitrov, D. et al. (2018) Global patterns of *Rhododendron* diversity: the role of evolutionary time and diversification rates. *Glob. Ecol. Biogeogr.* **27**, 913–924.
- Simao, F.A., Waterhouse, R.M., Ioannidis, P., Kriventseva, E.V. and Zdobnov, E. M. (2015) BUSCO: assessing genome assembly and annotation completeness with single-copy orthologs. *Bioinformatics*, **31**, 3210–3212.
- Smoot, M.E., Ono, K., Ruscheinski, J., Wang, P.L. and Ideker, T. (2011) Cytoscape 2.8: new features for data integration and network visualization. *Bioinformatics*, **27**, 431–432.
- Soza, V.L., Lindsley, D., Waalkes, A., Ramage, E., Patwardhan, R.P., Burton, J. N., Adey, A. et al. (2019) The *Rhododendron* genome and chromosomal organization provide insight into shared whole-genome duplications across the heath family (Ericaceae). *Genome Biol. Evol.* **11**, 3353–3371.
- Stamatakis, A. (2014) RAxML version 8: a tool for phylogenetic analysis and post-analysis of large phylogenies. *Bioinformatics*, **30**, 1312–1313.
- Sun, P., Schuurink, R.C., Caissard, J.C., Huguency, P. and Baudino, S. (2016) My way: noncanonical biosynthesis pathways for plant volatiles. *Trends Plant Sci.* **21**, 884–894.
- Tang, W., Sun, X.P., Yue, J.Y., Tang, X.F., Jiao, C., Yang, Y., Niu, X.L. et al. (2019) Chromosome-scale genome assembly of kiwifruit *Actinidia chinensis* with single-molecule sequencing and chromatin interaction mapping. *Gigascience*, **8**, giz027.
- Tarailo-Graovac, M. and Chen, N.S. (2009) Using RepeatMasker to identify repetitive elements in genomic sequences. *Curr. Protoc. Bioinformatics*, **4**, unit 4.10.
- Teh, B.T., Lim, K., Yong, C.H., Ng, C.C.Y., Rao, S.R., Rajasegaran, V., Lim, W.K. et al. (2017) The draft genome of tropical fruit durian (*Durio zibethinus*). *Nat. Genet.* **49**, 1633–1641.
- Wang, X.Y., Li, Z., Liu, B., Zhou, H., Elmongy, M.S. and Xia, Y.P. (2020) Combined proteome and transcriptome analysis of heat-primed azalea reveals new insights into plant heat acclimation memory. *Front. Plant Sci.* **11**, 1278.

- Wang, Y.P., Tang, H.B., DeBarry, J.D., Tan, X., Li, J.P., Wang, X.Y., Lee, T.H. *et al.* (2012) MScanX: a toolkit for detection and evolutionary analysis of gene synteny and collinearity. *Nucleic Acids Res.* **40**, e49.
- Wen, G.Z. (2017) A simple process of RNA-sequence analyses by Hisat2, Htseq and DESeq2. *Proceedings of the 2017 International Conference on Biomedical Engineering and Bioinformatics*, 11–15.
- Wu, H., Ma, T., Kang, M., Ai, F., Zhang, J., Dong, G. and Liu, J. (2019) A high-quality *Actinidia chinensis* (kiwifruit) genome. *Hortic. Res.* **6**, 117.
- Xia, E.H., Tong, W., Hou, Y., An, Y.L., Chen, L.B., Wu, Q., Liu, Y.L. *et al.* (2020) The reference genome of tea plant and resequencing of 81 diverse accessions provide insights into its genome evolution and adaptation. *Mol. Plant*, **13**, 1013–1026.
- Yang, F.S., Nie, S., Liu, H., Shi, T.L., Tian, X.C., Zhou, S.S., Bao, Y.T. *et al.* (2020) Chromosome-level genome assembly of a parent species of widely cultivated azaleas. *Nat. Commun.* **11**, 5269.
- Yang, Z.H. (2007) PAML 4: Phylogenetic analysis by maximum likelihood. *Mol. Biol. Evol.* **24**, 1586–1591.
- Zhang, C.F., Zhang, T.K., Luebert, F., Xiang, Y.Z., Huang, C.H., Hu, Y., Rees, M. *et al.* (2020a) Asterid phylogenomics/phylotranscriptomics uncover morphological evolutionary histories and support phylogenetic placement for numerous whole genome duplications. *Mol. Biol. Evol.* **37**, 3188–3210.
- Zhang, L.S., Chen, F., Zhang, X.T., Li, Z., Zhao, Y.Y., Lohaus, R., Chang, X.J. *et al.* (2020b) The water lily genome and the early evolution of flowering plants. *Nature*, **577**, 79–84.
- Zhang, L., Xu, P.W., Cai, Y.F., Ma, L.L., Li, S.F., Li, S.F., Xie, W.J. *et al.* (2017a) The draft genome assembly of *Rhododendron delavayi* Franch. var. *delavayi*. *Gigascience*, **6**, 1–11.
- Zhang, T.C., Qiao, Q., Novikova, P.Y., Wang, Q., Yue, J.P., Guan, Y.L., Ming, S. P. *et al.* (2019a) Genome of *Crucihimalaya himalaica*, a close relative of *Arabidopsis*, shows ecological adaptation to high altitude. *Proc. Natl. Acad. Sci. USA*, **116**, 7137–7146.
- Zhang, X., Zhang, S., Zhao, Q., Ming, R. and Tang, H. (2019b) Assembly of allele-aware, chromosomal-scale autopolyploid genomes based on Hi-C data. *Nat. Plants*, **5**, 833–845.
- Zhang, Y.H., Ni, J., Tang, F.P., Jiang, L.F., Guo, T.R., Pei, K.Q., Sun, L.F. *et al.* (2017b) The effects of different human disturbance regimes on root fungal diversity of *Rhododendron ovatum* in subtropical forests of China. *Canadian J. Forest Res.* **47**, 659–666.
- Zuker, A., Tzfira, T., Ben-Meir, H., Ovadis, M., Shklarman, E., Itzhaki, H., Forkmann, G. *et al.* (2002) Modification of flower color and fragrance by antisense suppression of the flavanone 3-hydroxylase gene. *Mol. Breeding*, **9**, 33–41.
- Figure S1** Evaluation of *Rhododendron ovatum* genome by k-mer analysis and read-depth.
- Figure S2** Genome-wide analysis of chromatin interactions in the *R. ovatum* genome based on Hi-C data.
- Figure S3** Genome assemblies of *R. ovatum* (ov) and *R. williamsianum* (wi).
- Figure S4** Types of gene duplication in the *R. ovatum* genome.
- Figure S5** Ks dot plot between *R. ovatum* and grape (*V. vinifera*).
- Figure S6** Ks dot plot between *R. ovatum* and kiwifruit (*A. chinensis*).
- Figure S7** Phylogenetic tree of *ERF* gene family.
- Figure S8** Phylogenetic tree of *MYB* gene family.
- Figure S9** Phylogenetic tree of *ANAC001* clade of *NAC* gene family.
- Figure S10** Chromosome localization of *NAC* genes of *R. ovatum*.
- Figure S11** Weighted gene co-expression network analysis (WGCNA) of the transcriptomes.
- Figure S12** Expression profiles of *HSP70s* and *TPSs* in response to different temperature treatments (25, 37, and 42 °C).
- Figure S13** Phylogenetic analysis and heat-induced expression profiles of *HSFs* in *R. ovatum*.
- Figure S14** Characteristics of tandem duplication in *R. ovatum* genome.
- Figure S15** GO functional enrichment network of tandem-duplicated genes.
- Figure S16** Tandem duplication ratio of the stress responsive genes.
- Figure S17** Expression profiles of *CYP450s* in different tissues.
- Figure S18** Phylogenetic tree of fatty acyl-ACP thioesterases coding genes.
- Figure S19** Statistic of *TPS* gene subfamilies.
- Figure S20** Phylogenetic tree of *TPSs* in *R. ovatum*.
- Figure S21** Phylogeny of the *TPS-a* subfamily.
- Figure S22** Phylogeny of the *TPS-b* subfamily.
- Figure S23** Phylogeny of the *TPS-c* subfamily.
- Figure S24** Phylogeny of the *TPS-e* subfamily.
- Figure S25** Phylogeny of the *TPS-f* subfamily.
- Figure S26** Phylogeny of the *TPS-g* subfamily.
- Figure S27** Chromosome localization of *RoTPS* genes.
- Figure S28** Expression profiles of *TPS* genes of *R. ovatum*.
- Figure S29** Structure features of the three alternative splicing transcripts of Ro_38431.
- Figure S30** Amino sequence alignment of Ro_38431.3 and Ro_43236.1.
- Figure S31** Expression profiles of adjacent genes of *TPS* clusters on chromosome 7.
- Table S1** Statistics for Illumina sequencing data of *R. ovatum* genome.
- Table S2** Statistics for PacBio sequencing data of *R. ovatum* genome.
- Table S3** Summary of contig-level genome assembly for *R. ovatum*.
- Table S4** BUSCO evaluation of the genomic completeness before and after elimination of redundancy.
- Table S5** Statistics for Hi-C sequencing data of *R. ovatum* genome.
- Table S6** Statistics for PacBio Iso-seq data of *R. ovatum*.
- Table S7** Gene prediction of *R. ovatum* genome.
- Table S8** Summary of repeat annotation of *R. ovatum*.
- Table S9** BUSCO evaluation of the genomic completeness of *R. ovatum*.
- Table S10** BUSCO evaluation of the gene prediction of *R. ovatum*.
- Table S11** Main flora volatiles compounds of *R. ovatum*.
- Data S1** Orthologous groups identified in these species.
- Data S2** Biological_process GO enrichment of expansive genes in *R. ovatum* compared to *R. delavayi* and *R. williamsianum*.
- Data S3** Full name list of the gene abbreviations.
- Data S4** *TPS* gene family of *R. ovatum*.
- Data S5** Pfam annotation of tandem-duplicated genes in *R. ovatum*.
- Data S6** Biological_process GO enrichment of tandem-duplicated genes in *R. ovatum*.